CONF-9509357--1

# Radiation Damage in Carbon-Carbon Composites:

## Structure and Property Effects

Timothy D. Burchell

Oak Ridge National Laboratory

Oak Ridge, Tennessee 37831-6088 U.S.A.

Subject Classification: 6180H, 8120N, 2852



E-mail: burchelltd@ornl.gov

## Abstract

Carbon-carbon composites are an attractive choice for fusion reactor plasma facing components because of their low atomic number, superior thermal shock resistance, and low neutron activation. Next generation tokamak reactors such as the International Thermonuclear Experimental Reactor (ITER), will require high thermal conductivity carbon-carbon composites and other materials, such as beryllium, to protect their plasma facing components from the anticipated high heat fluxes. Moreover, ignition machines such as ITER will produce a large neutron flux. Consequently, the influence of neutron damage on the structure and properties of carbon-carbon composite materials must be evaluated. Data from two irradiation experiments are reported and discussed here. Carbon-carbon composite materials were irradiated in target capsules in the High Flux Isotope Reactor (HFIR) at Oak Ridge National Laboratory (ORNL). A peak damage dose of 4.7 displacements per atom (dpa) at an irradiation temperature of ~600°C was attained. The carbon materials irradiated here included uni-directional, two-directional, and three-directional carbon-carbon composites. Irradiation induced dimensional changes are reported for the materials and related to single crystal dimensional changes through fiber and composite structural models. Moreover, carbon-carbon composite material dimensional changes are discussed in terms of their architecture, fiber type, and graphitization temperature. Neutron irradiation induced reductions in the thermal conductivity of two, three-directional carbon-

carbon composites are reported, and the recovery of thermal conductivity due to thermal annealing is demonstrated. Irradiation induced strength changes are reported for several carbon-carbon composite materials and are explained in terms of in-crystal and composite structural effects.

## 1. Introduction

Carbon materials have been used in nuclear fission reactors for more than 50 years. Indeed, the first nuclear core, constructed at the University of Chicago in the early 1940s, consisted of a stack or "pile" of graphite blocks. More recently, tokamak fusion devices have adopted carbon materials for their first wall linings, and for armor on their plasma facing components. For example, the Tokamak Fusion Test Reactor (TFTR) and DIIID in the U.S.A.; the Joint European Torus (JET), Tore Supra, and TEXTOR in Europe; and JT-60U in Japan make extensive use of carbon-carbon composites and fine-grained graphites as plasma facing materials. Carbon-carbon composites possess a number of attributes which make them an attractive choice for tokamak first wall, limiter and divertor armor (Fig. 1). These attributes include low atomic number, high thermal shock resistance, lack of a melting temperature (graphite sublimes at ~3600 K), and high thermal conductivity. Next generation tokamak fusion reactors such as the International Thermonuclear Experimental Reactor (ITER) will utilize carbon-carbon composite materials in their first wall or divertor armor. Plasma facing components in ITER must endure a severe environment, including high-heat fluxes, high armor surface temperatures, and eddy-current induced stresses which arise during plasma disruptions. Moreover, ITER will be an ignition machine and will thus produce a significant neutron flux from the deuterium-tritium fusion reaction. Therefore, plasma facing carbon-carbon composite materials will suffer structure and property degradation as a result of carbon atom displacements and crystal lattice damage,

caused by impinging high energy fusion neutrons and energetic helium ions from carbon transmutations. In a recent review of radiation damage in carbon materials, Burchell [1] calculated the neutron damage dose for the first wall of ITER to be ~0.1 displacements per atom (dpa) for the physics phase, and 2.7-8.2 dpa during the technology phase. Burchell's calculation included the moderation of neutrons, therefore allowing for a spectrum of neutron energies with the more damaging 3.5 and 8 MeV neutrons. Neutron irradiation damage studies reported here are in the dose range 1-5 dpa and thus are particularly relevant to the ITER technology phase.

The effects of neutron irradiation on graphite have been studied for the past fifty years. Graphite neutron damage induced structure and property changes are well understood [2,3], and recently comprehensive models have been developed to describe the irradiation induced structure and property changes in nuclear graphites [4]. Neutron irradiation causes the displacement of carbon atoms from their equilibrium lattice positions into interstitial locations, leaving vacancies in the basal planes (Fig. 2). Interstitial carbon atoms become increasingly mobile at higher temperatures, forming clusters and eventually new planes. Vacancies, which are only mobile at temperatures >400°C, form loops which eventually collapse. One consequence of neutron damage is a rapid increase in graphite strength and elastic moduli due to basal plane dislocation pinning. Subsequent changes in strength and elastic moduli occur due to changes in the polycrystalline structure of the graphite. A further consequence of neutron damage is a marked reduction in thermal conductivity. Irradiation defects act as phonon scattering centers and reduce the

phonon mean free path. In addition to physical property changes, graphites undergo dimensional and volume changes when irradiated. Initially, there is a volume shrinkage, but the shrinkage rate decreases and a reversal to growth occurs at higher doses. This effect is temperature dependent; above irradiation temperatures of ~600°C, increasing the irradiation temperature results in the reversal from shrinkage to growth occurring at lower neutron irradiation doses.

Recently, radiation damage in carbon-carbon composites has been reviewed [1] and materials property data for fusion reactor plasma facing carbon-carbon composites reported [5]. The limited amount of work on the effects of irradiation damage on carbon-carbon composites was highlighted. Gray [6] and Price [7] have reported the irradiation induced dimensional changes of carbon fibers. The fibers were observed to shrink along their length while the fiber diameter initially shrank and subsequently swelled. Burchell et al. [8] reported that two-directional (2D), carbon-carbon composites exhibited excessive swelling perpendicular to the fabric layers, in the range 22-37% growth, and shrank in directions parallel to the fabric layers, typically 3-19%, on irradiation at 400°C to approximately 4 dpa.

Carbon-carbon composites are an infinitely variable family of materials. Processing and design variables (Fig. 3)—such as: (1) architecture, i.e., uni-directional (1D), two-directional (2D), three-directional (3D), or random fiber distribution; (2) fiber precursor, i.e., pitch, polyacrylonitrile (PAN), or vapor-grown; (3) matrix precursor, i.e., liquid impregnation (pitch or resin) or CVI; and (4) final heat treatment (graphitization) temperature—will influence the properties and

behavior of carbon-carbon composites. In order to select a carbon-carbon composite for a PFC application in which neutron damage will be significant, we must understand the effect of processing variables on neutron irradiation induced structure and property changes.

Recognizing the need to elucidate these effects, Burchell et al. [9] irradiated 1D, 2D, and 3D carbon-carbon composites at 600°C and to damage doses up to 1.5 dpa. Three-directional carbon-carbon composites were shown to exhibit more isotropic dimensional changes than either 1D or 2D carbon-carbon composite materials. Pitch fiber composites were shown to be more dimensionally stable than PAN fiber composites and high final heat-treatment (graphitization) temperatures were found to be beneficial. Here we report an extension of Burchell et al.'s study to higher damage doses. Dimensional, strength and thermal conductivity changes are reported for 1D, 2D, and 3D carbon-carbon composites irradiated to a peak neutron dose of 4.7 dpa at an irradiation temperature of 600°C.

## 2. Experimental

### 2.1 Materials

Neutron irradiation experiments were conducted on a series of carbon-carbon composites. The 1D carbon fiber composite (UFC) was a PAN derived fiber composite manufactured by Fiber Materials, Inc. in the U.S.A. Random (chopped) fiber composite (RFC) and A05 were 2D, PAN fiber composites manufactured by Fiber Materials, Inc., U.S.A. and Carbone Lorraine, France, respectively. Two, 3D carbon-carbon composites were used. Fiber Materials, Inc.'s

223 and 222, which were, respectively, PAN fiber and pitch fiber composite materials. In addition to the carbon-carbon composites, a reference grade nuclear graphite (H-451) was included in the irradiation experiments. Selected composites were heat-treated at 2650 or 3100°C prior to inclusion in the irradiation capsules. The materials, and their heat treatment condition, are summarized in Table 1.

### 2.2 Irradiation Conditions

Irradiations were performed in the target region of the High Flux Isotope Reactor (HFIR) at the Oak Ridge National Laboratory (ORNL). The irradiation capsules, designated HTFC-I and -II, were neon gas filled and the specimen temperature was controlled by sizing the annular gap between the specimen and the capsule. Silicon carbide temperature monitors were placed at intervals throughout the capsule. The irradiation specimens were either hollow cylinders, 6.35-mm long with an inside diameter of 3.18 mm, or solid cylinders of 12-mm nominal outside diameter and lengths ranging from 6 to 12 mm. A maximum neutron dose of 2.44 $\times 10^{25}$ n/m$^2$ [E > 50 keV] or 1.6 dpa, and 7.28 $\times 10^{25}$ n/m$^2$ [E > 50 keV] or 4.7 dpa, was attained for HTFC-I and -II, respectively, at an irradiation temperature of 600°C.

### 2.3 Determination of Property Changes

Pre- and post-irradiation characterization included dimensional measurement, brittle ring strength and thermal conductivity. Pre-irradiation control specimens were cut from adjacent locations in the carbon-carbon composite billets.

Brittle ring strength was calculated using the formula

$$\sigma = \frac{6K_t P(D_2 + D_1)}{\pi t(D_2 - D_1)^2} \text{ [Pa]} \qquad (1)$$

where $K_t$ is the stress intensity factor, equal to 1.25 for the ring geometry used here, P is the load at failure (N), $D_2$ is the outside diameter (m), $D_1$ is the inside diameter (m), and t is the ring thickness (m). Thermal conductivity was calculated from the thermal diffusivity (measured by the thermal pulse technique) using the formula

$$K = \alpha \cdot \rho \cdot C_p \qquad (W/m \cdot K) \qquad (2)$$

where $\alpha$ is the thermal diffusivity ($m^2/s$), $\rho$ is the specimen density ($kg/m^3$), and $C_p$ is the specific heat ($J/kg \cdot K$). The thermal diffusivity measurements were made on irradiated and unirradiated specimens over the temperature range 100-1600°C.

## 3. Results

### 3.1 Dimensional and Volume Changes

The neutron irradiation induced dimensional changes of our reference graphite (H-451), a 1D, carbon-carbon composite (UFC), and the two-directional carbon-carbon composites A05 and RFC are shown in Fig. 4 (specimen length) and Fig. 5 (diameter change), respectively. The dimensional changes are expressed as percent shrinkage or growth from the specimens pre-irradiation dimensions, and are plotted as a function of neutron dose in displacements per atom (dpa). Figure 6 shows the volume changes for specimens of H-451, UFC, RFC, and A05. Figures

7 and 8 show the neutron irradiation induced diameter and length changes, respectively, for H-451 and two, 3D carbon-carbon composites (222 and 223). Data are reported for the 223 and 222 composites in the 2650 and 3000°C heat treatment conditions. Volume changes for the 222 and 223 composites, and for comparison, H-451 reference grade graphite, are shown in Fig. 9.

### 3.2 Thermal Conductivity

Thermal conductivity as a function of temperature for a 3D carbon-carbon composite (222) in the unirradiated, irradiated, and irradiated and annealed condition are shown in Fig. 10. In this instance, the specimen was irradiated to a peak dose of 4.2 dpa. Similar data for the PAN fiber 3D carbon-carbon composite (223), irradiated to a peak dose of 4.6 dpa, are reported in Fig. 11. Additional data were obtained for specimens of 222 and 223 composites irradiated to peak doses ranging from 1 to 4.5 dpa. In all cases, the temperature dependency of the thermal conductivity was similar for the three conditions, i.e., unirradiated—thermal conductivity decreases with increasing measurement temperature in the range 25 to 1600°C (Fig. 11); irradiated—thermal conductivity increased with increasing measurement temperature, particularly above the irradiation temperature of 600°C; irradiated and annealed—thermal conductivity increased with decreasing temperature, exhibiting a similar temperature dependency as the unirradiated case.

### 3.3 Strength

Brittle ring strength data for H-451 graphite and carbon-carbon composites RFC, UFC, 222, and 223 irradiated to doses up to approximately 2.5 dpa are shown

in Figs. 12 and 13. Data for the 3D composites, 222 and 223, were measured on specimens heat treated at 2650 or 3100°C prior to irradiation (Fig. 13).

## 4. Discussion

### 4.1 Irradiation Induced Dimensional Changes

Neutron irradiation induced dimensional changes for three of the PAN fiber composite materials studied here are summarized in Fig. 14. Specimen length and diametral changes are shown for a 1D composite (UFC), a 2D composite (RFC), and a 3D composite (223). The 1D composite exhibited extremely anisotropic dimensional changes, undergoing rapid shrinkage in the fiber-axis direction (length). In the direction perpendicular to the fiber axis (diameter) the composite shrank at a dose $\leq$1 dpa, followed by a reversal to expansion, returning to zero dimensional change at approximately 2.5 dpa and continuing to expand at an increasing rate. A similar trend was observed for the 2D composites, as typified by the RFC material (Fig. 14), where the fiber axis is in the specimen diametral direction. In the of-axis direction (length) the composite exhibited a slight contraction followed by expansion, returning to the original length at approximately 2 dpa. The diametral (fiber-axis) directions of the RFC specimens exhibited shrinkage, although the magnitude of the shrinkage was much less for the same damage dose than in the case of the 1D composite. In contrast to the 1D and 2D composites, the 3D PAN fiber composite exhibited isotropic behavior at damage doses up to approximately 2 dpa. At doses exceeding 2 dpa, the composite z-direction

(specimen length) continued to display shrinkage, whereas the fiber x-y (specimen diameter) direction exhibited reversal and slight growth.

Interpretation of the irradiation-induced dimensional changes of carbon-carbon composite materials requires: (1) an understanding of the graphite single crystal dimensional changes; (2) a microstructural model of the carbon fibers used in the composite (PAN fibers in all three materials in Fig. 14); and (3) knowledge of the composite architecture and the interactions of the fiber, fiber bundle, matrix, and porosity in the composite. As described in the introduction, the mechanism of neutron damage in the graphite crystal is well understood. Figure 2 shows an illustration of the mechanism of neutron displacement damage. The graphite crystal lattice undergoes expansion in the <c> direction (perpendicular to the graphite layer planes) and shrinkage in the two <a> directions (parallel to the layer planes). Several models of the microstructure of PAN fibers have been suggested [10]. Pennock et al. [11] have reported the structure of pitch-based carbon fibers, and typical pitch fiber structures are shown in Fig. 15. A "core-sheath" model of a PAN carbon fiber similar to that described by Bennett and Johnson [12] is shown in Fig. 16. In the core sheath model, the graphitic layer planes are arranged circumferentially in the fiber periphery and radially at the core of the fiber. Therefore, in the sheath region the preferred crystallographic <c> direction is perpendicular to the fiber axis (radial) and the two crystallographic <a> directions are circumferential and axial (Fig. 16). Applying the known graphite crystal irradiation induced dimensional changes to the fiber microstructural models in

Figs. 15 and 16, we would predict the fiber behavior to be dominated by shrinkage in the <a> direction, resulting in both fiber axial and diameteral shrinkages. Expansion of the fiber in the <c> direction, and diameteral <a> shrinkage, may be initially accommodated by the interplaner voids or pores in the fiber, or by the extensive network of cracks known to exist within the carbon-carbon composite, such as those within the fiber bundles or at the fiber bundle-matrix interface.

The influence of composite architecture is evident from a comparison of the irradiation-induced dimensional behavior of 1D and 2D PAN fiber, carbon-carbon composite materials (Fig. 14). In the 1D material the PAN fibers are aligned along the specimen axis (Fig. 16). The composite would thus be expected to shrink along the fiber axis (length) direction upon irradiation due to fiber axial shrinkage. In the diametral direction (perpendicular to the fiber-axis) we would predict an initial shrinkage, followed by a reversal to growth, as the internal porosity in filled by the fiber <c> direction growth. Behavior of this nature is clearly displayed by the 1D carbon-carbon composite (Figs. 4, 5, and 14). In the 2D, random-fiber composite (RFC) material, the PAN fibers are oriented randomly in one plane, but are all perpendicular to the axis of the irradiation specimen (Fig. 18). The dominant <a> axis shrinkage of the fiber under neutron irradiation will thus cause shrinkage in the specimen diametral direction; whereas in the axial direction, the specimen should mimic the fiber diametral behavior, initially shrinking, followed by turnaround to growth—as indicated by the data plotted in Figs. 4, 5, and 14.

In 3D carbon-carbon composite specimens, irradiation-induced shrinkage in both diametral and length directions would be predicted due to x, y, and z direction fiber axial shrinkage. Clearly this was observed, as shown by our data in Figs. 7, 8, and 14, up to doses of ~3 dpa. At higher neutron doses the complex interaction between fiber axial shrinkage, fiber diametral growth, porosity, and matrix behavior will cause a turnaround to growth, as seen for the 223 material's volume change data (Fig. 9). The damage dose at which volume turnaround will occur for a particular composite will depend upon several factors, such as the distribution of fiber, i.e., the fiber volume fraction in each of the three fiber directions, the amount and distribution of the porosity in the material, the fiber type, structure, and crystallinity, and the matrix structure, crystallinity, and irradiation dimensional behavior. In the 3D PAN fiber composite material (223) reported here, the turnaround to growth began in the x-y (diametral) direction at approximately 2-3 dpa, whereas in the z (length) direction turnaround did not occur at doses up to 5 dpa (Figs. 8, 9, and 14). It is postulated that this irradiation shrinkage anisotropy is the result of an unbalanced fiber distribution, and/or the presence of more accommodating porosity along the x- or y-fiber/matrix interfaces than along the z-fiber/matrix interface.

The influence of fiber structure and crystallinity on the irradiation-induced dimensional change of two, 3D carbon-carbon composite materials is shown in Fig. 19. In Fig. 19(a) the dimensional changes of a pitch fiber (222) and a PAN fiber (223) 3D composites in the z-fiber direction (specimen length) are shown. The

pitch fiber composite exhibited less shrinkage for the same neutron dose than the PAN fiber composite. The superior behavior of the pitch fiber composite is attributed to the greater degree of crystallinity in pitch fibers [13]. The data in Fig. 19(b) indicate that increasing the final heat-treatment temperature reduces the magnitude of dimensional change in a 3D PAN fiber, carbon-carbon composite. The relationship between increased crystallinity or increased final heat treatment temperature and reductions in the magnitude of neutron irradiation induced dimensional change has been clearly demonstrated in studies of the irradiation behavior of pyrolytic graphites [1, 14]. In this, and previous studies of irradiation damage [9], we have shown that composites manufactured from more crystalline pitch fibers, or that have been graphitized at high temperatures (>3000°C), exhibit less dimensional change at a given dose than carbon-carbon composites manufactured from less crystalline PAN fibers or graphitized at lower temperatures (<2700°C).

### 4.2 Effect of Neutron Dose on Thermal Conductivity

Thermal conductivity is a key physical property for plasma facing materials. Degradation of thermal conductivity due to neutron damage will result in higher surface armor temperatures and hence greater surface losses due to sputtering and erosion processes. The effect of neutron damage on high temperature thermal conductivity is therefore of considerable interest. Here, we shall limit our discussion to the two, 3D carbon-carbon composite (223 PAN fiber and 222 pitch

fiber) materials. The temperature dependence of thermal conductivity is shown for 222 (pitch) and 223(PAN) composites in Figs. 10 and 11, respectively. For both composites the thermal conductivity is measured in the z-fiber bundle direction. A comparison of Figs. 10 and 11 indicates that the 222 (pitch fiber) composite has a greater thermal conductivity prior to irradiation, which is attributed to the higher crystallinity and consequent longer phonon mean free path in the pitch fiber (222) material. Both the 222 and 223 composites suffer severe degradation of thermal conductivity after irradiation to >4 dpa. At the temperature of irradiation (~600°C) the reduction was between 50 and 60%. The thermal conductivity of the irradiated samples increased with temperature, which was in direct contrast to the unirradiated specimens. The increasing thermal conductivity was attributed to thermal annealing of irradiation-induced defects which act as phonon-phonon scattering centers. At higher measurement temperatures the irradiated and unirradiated specimen data sets converge as increasing amounts of the displacement damage are annealed. Post annealing (cooldown) thermal conductivity curves are also shown in Figs. 10 and 11, revealing the extent of recovery of thermal conductivity. At the irradiation temperature, the post annealing thermal conductivity was reduced by as little as 20% of the unirradiated conductivity. The effects of irradiation and post-irradiation annealing on the thermal conductivity, as a function of neutron dose, are shown for the 222 (pitch fiber) composite in Fig. 20. The thermal conductivity at the irradiation temperature is reduced to approximately 60% of the unirradiated value at doses as low as ~1 dpa, but the reduction

saturates and is relatively constant over the dose range 1 to 4.5 dpa. At larger damage doses than shown in Figs. 20 and 21, the thermal conductivity would be expected to eventually degrade due to severe irradiation-induced structural changes (break-up) of the composite material. The extent to which thermal conductivity is recovered after thermal annealing at 1600°C is also shown in Fig. 20 where post-annealing thermal conductivity is only 20-30% less than the unirradiated thermal conductivity at the irradiation temperature. Similar data were obtained for the 223 PAN fiber material. The degree to which irradiation-induced losses of thermal conductivity may be recovered in carbon-carbon composites is particularly significant to the design of next-generation tokamaks such as ITER, where plasma disruptions may cause high plasma-facing component surface temperatures and hence beneficial thermal annealing and recovery of thermal conductivity. Low dose neutron irradiation effects on the thermal conductivity of carbon-carbon composites have been reported by Thiele et al. [15]. They showed that the thermal conductivity, measured at the irradiation temperature (600°C), reduced by ~20-40% at neutron dose up to 0.1 dpa. Thiele's data are shown in Fig. 21 along with our data for A05 ($\perp$) at ~1 dpa. At ~1 dpa the thermal conductivity is further reduced, giving a fractional reduction in thermal conductivity [1 - ($K/K_o$)] of >0.5. This compares favorably with our data in Fig. 20, for the 222 three-directional composite, which shows that thermal conductivity has saturated at dose >1.3 dpa. Evidently, thermal conductivity degradations at 600°C can be expected to saturate at ~1.0 dpa and remain unchanged until the dose exceeds ~5 dpa.

As reviewed by Burchell [1], low temperature (<200°C) irradiation of carbon-carbon composites can be expected to cause even more severe reductions in thermal conductivity than reported here for 600°C irradiations. Moreover, the build-up of Wigner energy can be expected. Potentially, Wigner energy could accumulate in the cooler parts (<100°C) of a water-cooled ITER divertor armored with carbon-carbon composites. Wigner energy levels can be controlled through the annealing process, which additionally restores much of the thermal conductivity. However, the possible build-up of Wigner energy in carbon-carbon composite plasma-facing materials must be properly addressed in the design process.

### 4.3 Effect of Neutron Dose on Strength

The influence of neutron irradiation on the strength of H-451 graphite and carbon-carbon composite materials UFC, RFC, 222, and 223 are reported in Figs. 12 and 13. With the exception of the 223 (heat treated at 2650°C prior to irradiation) strength increased with increasing neutron damage up to doses of ~2.5 dpa. Increasing strength with neutron irradiation is well known for graphites [1-3, 14] and is attributable to: (1) pinning of basal plane dislocations by irradiation-induced defects in the graphite crystallites and (2) the reduction of internal porosity due to irradiation-induced volume shrinkage (densification). The pitch fiber based, 3D carbon-carbon composite (222) exhibited a clear trend for increasing strength with neutron damage dose (Fig. 13). Moreover, the higher final heat treatment temperature has lessened the degree to which the strength is increased in the case

of the 222 (3100°C) material. Inspection of the volume change data for these two materials (Fig. 9) indicates that they undergo similar amounts of densification. The strength differences between the 222 (2650°C) and the 222 (3100°C) materials are thus more correctly attributed to differences in fiber crystallinity. Specifically, the high graphitization temperature would be expected to result in a lower initial concentration of lattice defects and thus fewer dislocation pinning sites. The PAN fiber-based, 3D carbon-carbon composite (223) showed an increase in strength up to ~1 dpa followed by a decrease in strength to levels similar to the unirradiated strength at ~2.5 dpa. Reductions in the strength of graphite at higher doses have been reported for graphites [1-3, 14, 16] and are associated with volume shrinkage turnaround to growth, i.e., the formation of new cracks as the material begins to swell. However, the volume change data for 223 indicates no evidence of turnaround at doses <2.5 dpa, although turnaround onset appears to occur at doses >3 dpa. A possible explanation of this discrepancy is the probable weakening and/or cracking of the fiber-matrix interface at relatively low neutron damage doses due to fiber axial shrinkage. The contribution of matrix-fiber interface cracks to the volume turn-around behavior would be minimal, but their deleterious influence on strength would be expected to be very significant.

Increases in carbon-carbon composite materials strength after irradiation have been reported by others. Sato et al. [17] irradiated two composite materials at a temperature of ~800°C and to a peak damage dose of 1.1 dpa. Both materials exhibited compressive strength increases >20%. Tanabe et al. [18] have reported

the mechanical properties of a 1D, PAN fiber, carbon-carbon composite material irradiated at 240 and 600°C to 0.64 and 0.87 dpa, respectively. Strength and failure strain both increased after irradiation. The data reported here, and by others [17, 18], clearly show that at neutron doses up to ~2 dpa and irradiation temperatures in the range 240-800°C the strength of carbon-carbon composites can be expected to increase—in some cases by more than 20%.

## 5.0 Conclusions

A series of carbon-carbon composite materials have been irradiated in the HFIR at ~600°C to a peak neutron damage dose of 4.7 dpa. Dimensional and volume changes have been analyzed in terms of architecture, reinforcing fiber precursor, and final graphitization temperature. The dimensional change behavior can be interpreted through composite structural models, a fiber microstructural model, and the expected single crystal dimensional changes.

The data reported here showed that 3D composite materials behaved more isotropically than 2D materials or 1D materials. Pitch fiber composites are more dimensionally stable than PAN fiber composites, and a high final heat-treatment (graphitization) temperature was seen to be beneficial, particularly with respect to minimizing the dimensional changes of a PAN fiber carbon-carbon composite. With the exception of the pitch derived fiber 222 composite, all of the carbon-carbon composites examined here underwent shrinkage reversal or "turnaround" in one specimen dimension (length or diameter). The 2D composites, A05 and RFC,

exhibited "turnaround" behavior in their specimen length direction ($\perp$ to fiber axis) while the 1D composite, UFC, exhibited marked turnaround in the diameteral direction ($\perp$ to fiber axis), but continued to shrink in the length ($\parallel$ to fiber axis) direction. It is concluded that these effects are a consequence of the dominant role of the carbon fiber in the neutron irradiation induced dimensional change mechanism of carbon-carbon composite materials.

The thermal conductivity of carbon-carbon composite materials was severely degraded by neutron irradiation, reducing exponentially to about 40-50% of its unirradiated value with doses up to ~1 dpa. Above ~1 dpa the thermal conductivity saturates and remains constant at doses up to at least 4.5 dpa. Post-irradiation annealing to 1600°C causes a recovery of thermal conductivity to approximately 80% of the unirradiated value at the irradiation temperature. The extent to which thermal conductivity can be recovered is particularly significant to the design of plasma-facing components for next-generation fusion devices.

The strength of the carbon-carbon composites increased on neutron irradiation to damage doses of ~4.7 dpa. The 3D, PAN derived fiber composite was an exception, and exhibited a maximum in strength at ~1 dpa. This was attributed to the formation of fiber-matrix interface cracks at low doses.

**Acknowledgements:** Research sponsored by the Office of Fusion Energy, U.S. Department of Energy, under contract DE-AC05-84OR21400 with Lockheed Martin Energy Systems Inc. The author wishes to acknowledge the assistance of Mr. J. P. Strizak for conducting the strength measurements.

## References


1. Burchell, T. D., "Radiation Damage in Carbon Materials," in "Physical Processes of the Interaction of Fusion Plasmas with Solids" (Edited by W. Hofer and J. Roth) (Academic Press, Inc., New York 1995) Chpt. 10.
2. Simmons, J. W. H., "Radiation Damage in Graphite (Pergamon Press, Oxford 1965).
3. Nightingale, R., "Nuclear Graphite" (Academic Press, New York 1962).
4. Kelly, B. T. and Burchell, T. D., CARBON **32**, 499 (1994).
5. Burchell T. D. and Oku, T., "Materials Properties Data for Fusion Reactor Plasma Facing Carbon-Carbon Composites," Nuclear Fusion—Atomic and Plasma-Materials Interactions Data for Fusion **5**, 77 (International Atomic Energy Agency, Vienna 1994).
6. Gray, W. J., BNWL Report 2390 (Battelle Pacific Northwest Laboratories, Richland, Washington 1970).
7. Price, R. J., Hopkins, R. J., and Engle, G. B., in Proceedings 17th Biennial Conference on Carbon, p. 340 (American Carbon Society 1985).
8. Burchell, T. D., Eatherly, W. P., Hollenburg, G. W., Slagle, D. D., and Watson, R. D., in Proceedings 20th Biennial Conference on Carbon, p. 598 (American Carbon Society 1991).
9. Burchell, T. D., Eatherly, W. P., Robbins, JM, and Strizak, J. P., J. Nucl. Mater. **191-194**, 295 (1992).

10. Donnet, J. B. and Bansal, R. C., Carbon Fibers, 2nd Ed., (Dekker, New York, 1990).

11. Pennock, G. M., Taylor, G. H., and Fitzgerald, J. D., CARBON **31**, 586 (1993).

12. Bennett, S. C. and Johnson, D. L., CARBON **17**, 25 (1979).

13. Bright, A. A. and Singer, L. S., CARBON **17**, 59 (1979).

14. Engle, G. B. and Eatherly, W. P., High Temperature-High Pressure **4**, 119 (1972).

15. Thiele, B. A., Binkle, L., Koizlik, K., and Nickel, H., in Effects of Radiation on Materials: 16th International Symposium, ASTM **1175**. (Edited by A. S. Kumar, D. S. Gelles, R. K. Nanstad, and E. A. Little) (American Society for Testing and Materials, Philadelphia 1993) p. 1304.

16. Burchell, T. D. and Eatherly, W. P., J. Nucl. Mater. 179-181, **205** (1991).

17. Sato, S., Kuramada, A., Kawamata, K., Ishida, R., Fusion Engineering and Design **13**, 159 (1990).

18. Tanabe, Y., et al., CARBON **29**, 905 (1991).

**Table I. Summary of Materials Included in ORNL Irradiation Experiments HTFC I and II**

| Designation | Description | Heat treatment condition |
|---|---|---|
| H-451 | Near-isotropic nuclear graphite (reference material). | As received |
| A05 | Carbone Lorraine. 2D carbon-carbon composite. PAN fibers. | As received |
| UFC | Fiber Materials, Inc. 1D fiber composite. PAN fibers. | 3100°C |
| RFC | Fiber Materials, Inc. Random fiber composite. PAN fibers (chopped). | As received |
| 223 | Fiber Materials, Inc. 3D fiber composite. PAN fibers. | 2650 and 3100°C |
| 222 | Fiber Materials, Inc. 3D fiber composite. Pitch fibers (P55). | 2650 and 3100°C |

**Figure Captions**

1. The major plasma facing components of a tokamak fusion device.
2. The mechanism of irradiation damage in the graphite crystal lattice.
3. Flow diagram for the carbon-carbon composite manufacturing process.
4. Neutron irradiation induced length changes of UFC, RFC, and A05 carbon-carbon composites and H-451 graphite irradiated at 600°C.
5. Neutron irradiation induced diameter changes of UFC, RFC, and A05 carbon-carbon composites and H-451 graphite irradiated at 600°C.
6. Neutron irradiation induced volume changes of UFC, RFC, and A05 carbon-carbon composites and H-451 graphite irradiated at 600°C.
7. Neutron irradiation induced diameter changes of 3D carbon-carbon composites 222 and 223, and H-451 graphite irradiated at 600°C.
8. Neutron irradiation induced length changes of 3D carbon-carbon composites 222 and 223, and H-451 graphite irradiated at 600°C.
9. Neutron irradiation induced volume changes of 3D carbon-carbon composites 222 and 223, and H-451 graphite irradiated at 600°C.
10. The temperature dependence of thermal conductivity of 222 3D carbon-carbon composite in the unirradiated, irradiated, and irradiated-annealed condition (irradiation conditions: 4.2 dpa at 600°C).
11. The temperature dependance of thermal conductivity of 223 3D carbon-carbon composite in the unirradiated, irradiated, and irradiated-annealed conditions (irradiation conditions: 4.6 dpa at 600°C).

12. The influence of neutron irradiation on the brittle ring strength of H-451 graphite, and carbon-carbon composites UFC and RFC irradiated at 600°C.

13. The influence of neutron irradiation on the brittle ring strength of 3D carbon-carbon composites 222 and 223, heat-treated at 2650 or 3100°C and irradiated at 600°C.

14. Neutron irradiation induced dimensional changes of several carbon-carbon composites irradiated at 600°C.

15. Pitch carbon fiber structural model and orientation of crystallographic basal planes.

16. PAN carbon fiber structural model and orientation of graphite crystallographic planes.

17. A microstructural interpretation of irradiation induced dimensional changes in a 1D carbon-carbon composite.

18. A microstructural interpretation of irradiation induced dimensional changes in a 2D carbon-carbon composite.

19. Irradiation induced dimensional changes in two, 3D carbon-carbon composites: (a) a comparison of pitch and PAN fiber composite behavior, and (b) the effect of heat treatment temperature on the dimensional change of a PAN (223) carbon-carbon composite.

20. The effect of post irradiation annealing on the thermal conductivity of a pitch fiber, 3D carbon-carbon composite (222).

21. A comparison of low dose neutron irradiation effects on the thermal conductivity of several carbon-carbon composites from Thiele et al. [15] and ORNL experiment HTFC I.

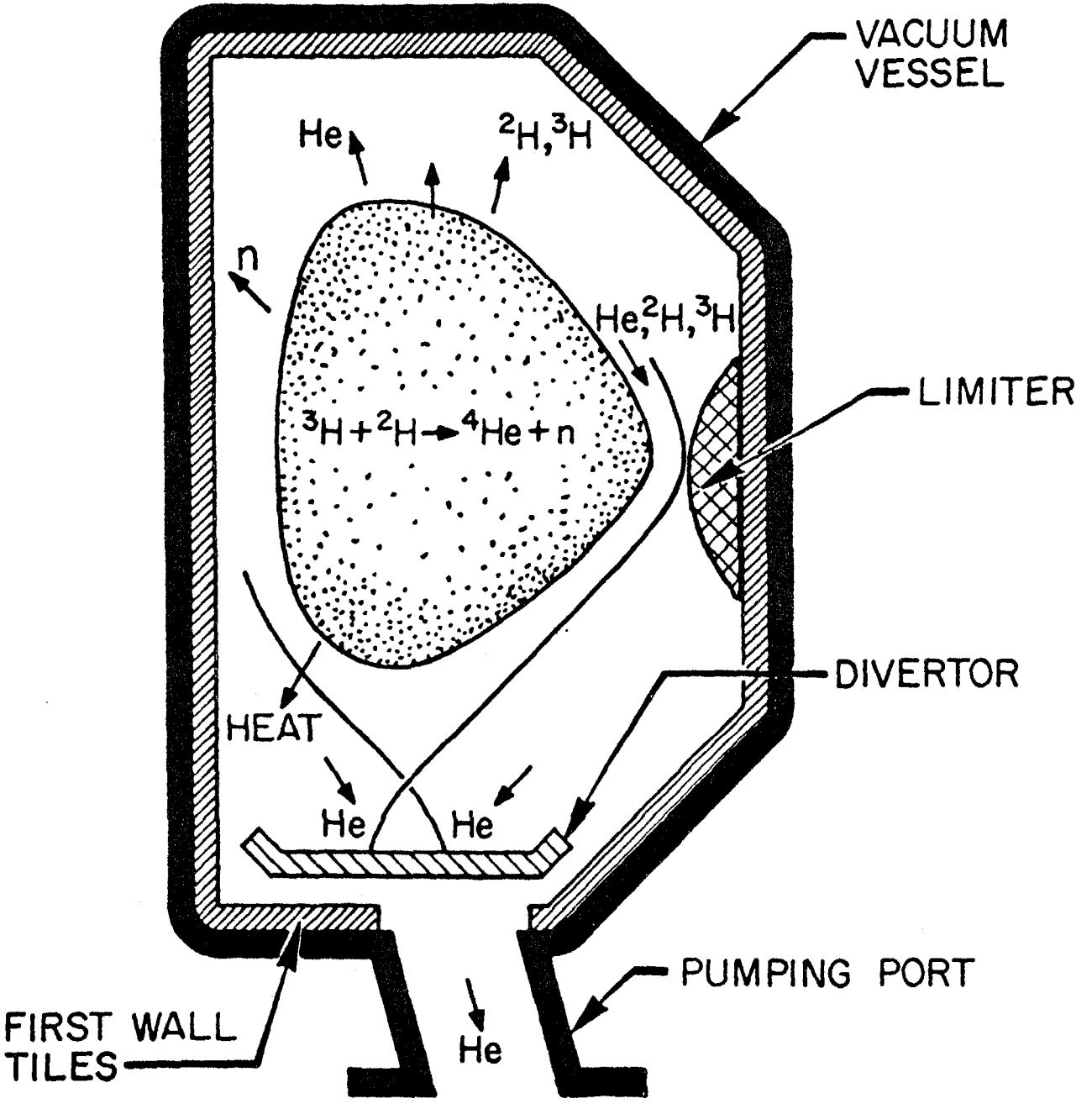
VACUUM
VESSEL
He
$^2H, ^3H$
n
He, $^2H$, $^3H$
LIMITER
$^3H + ^2H \rightarrow ^4He + n$
DIVERTOR
HEAT
He
He
PUMPING PORT
FIRST WALL
TILES
He

Fig. 1

# RADIATION DAMAGE IN GRAPHITE

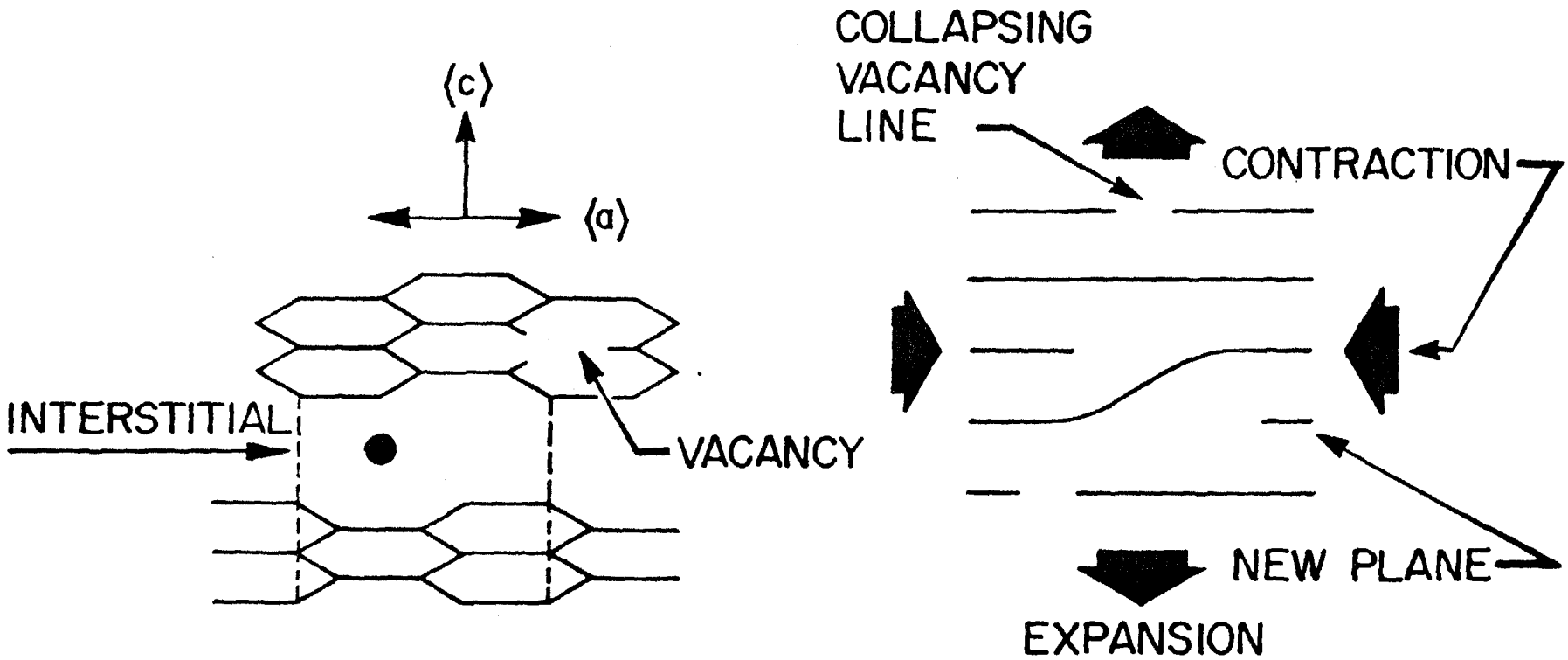


Fig. 2

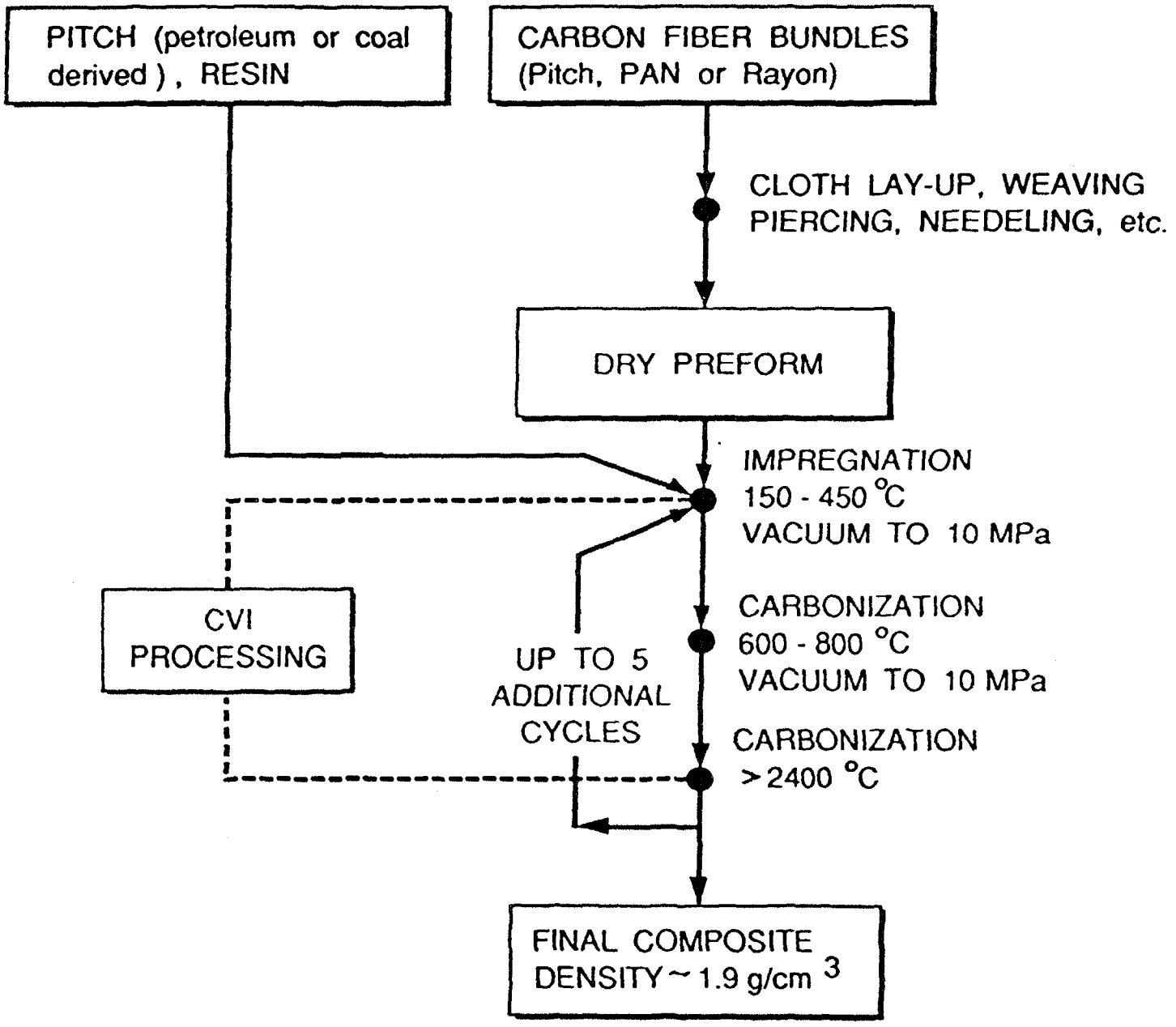
PITCH (petroleum or coal derived ), RESIN
CARBON FIBER BUNDLES (Pitch, PAN or Rayon)
CLOTH LAY-UP, WEAVING PIERCING, NEEDELING, etc.
DRY PREFORM
IMPREGNATION 150 - 450 °C VACUUM TO 10 MPa
CARBONIZATION 600 - 800 °C VACUUM TO 10 MPa
CARBONIZATION >2400 °C
CVI PROCESSING
UP TO 5 ADDITIONAL CYCLES
FINAL COMPOSITE DENSITY ~ 1.9 g/cm 3

Fig. 3

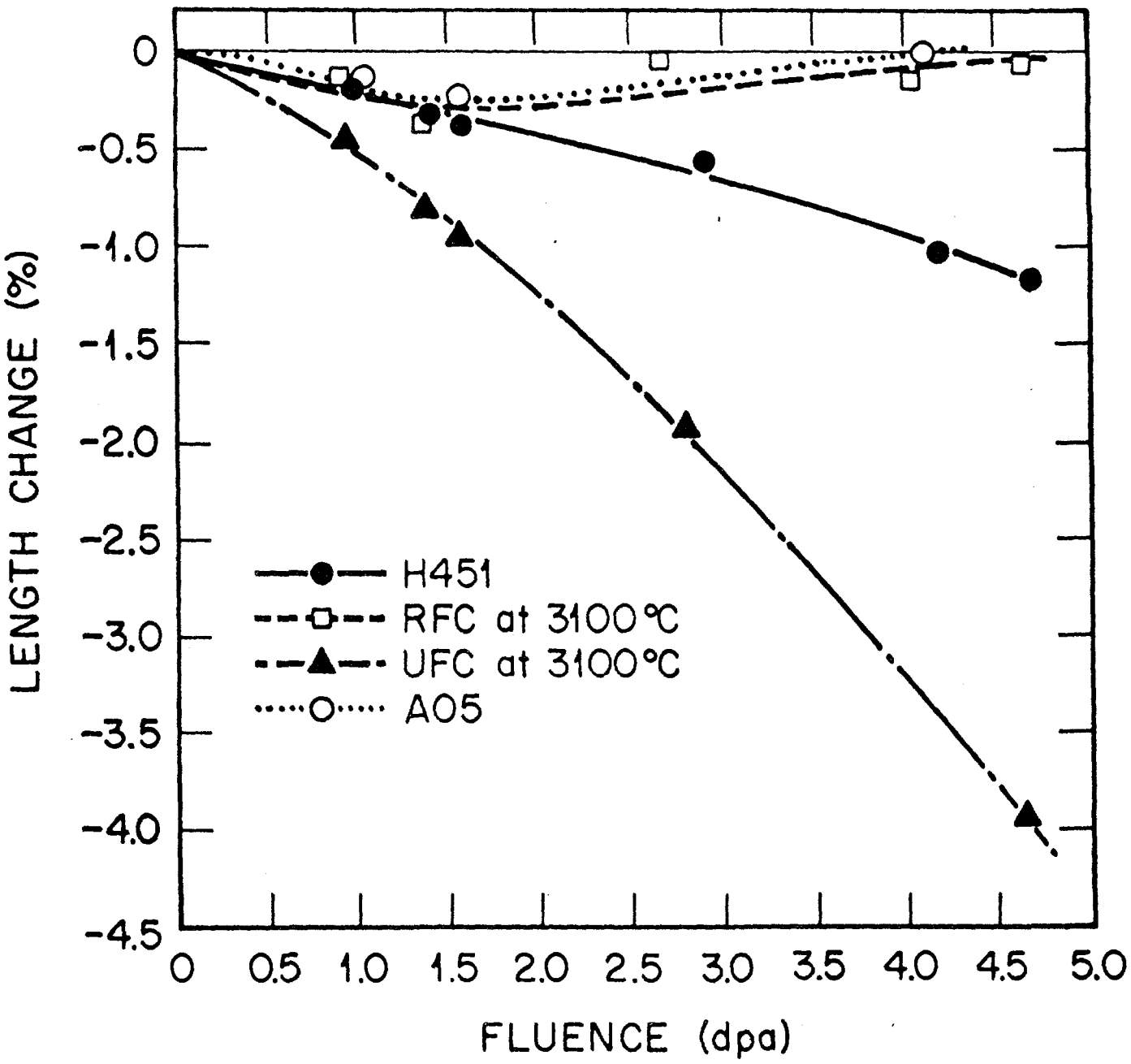
LENGTH CHANGE (%)
0
-0.5
-1.0
-1.5
-2.0
-2.5
-3.0
-3.5
-4.0
-4.5
H451
RFC at 3100°C
UFC at 3100°C
A05
0
0.5
1.0
1.5
2.0
2.5
3.0
3.5
4.0
4.5
5.0
FLUENCE (dpa)

Fig. 4

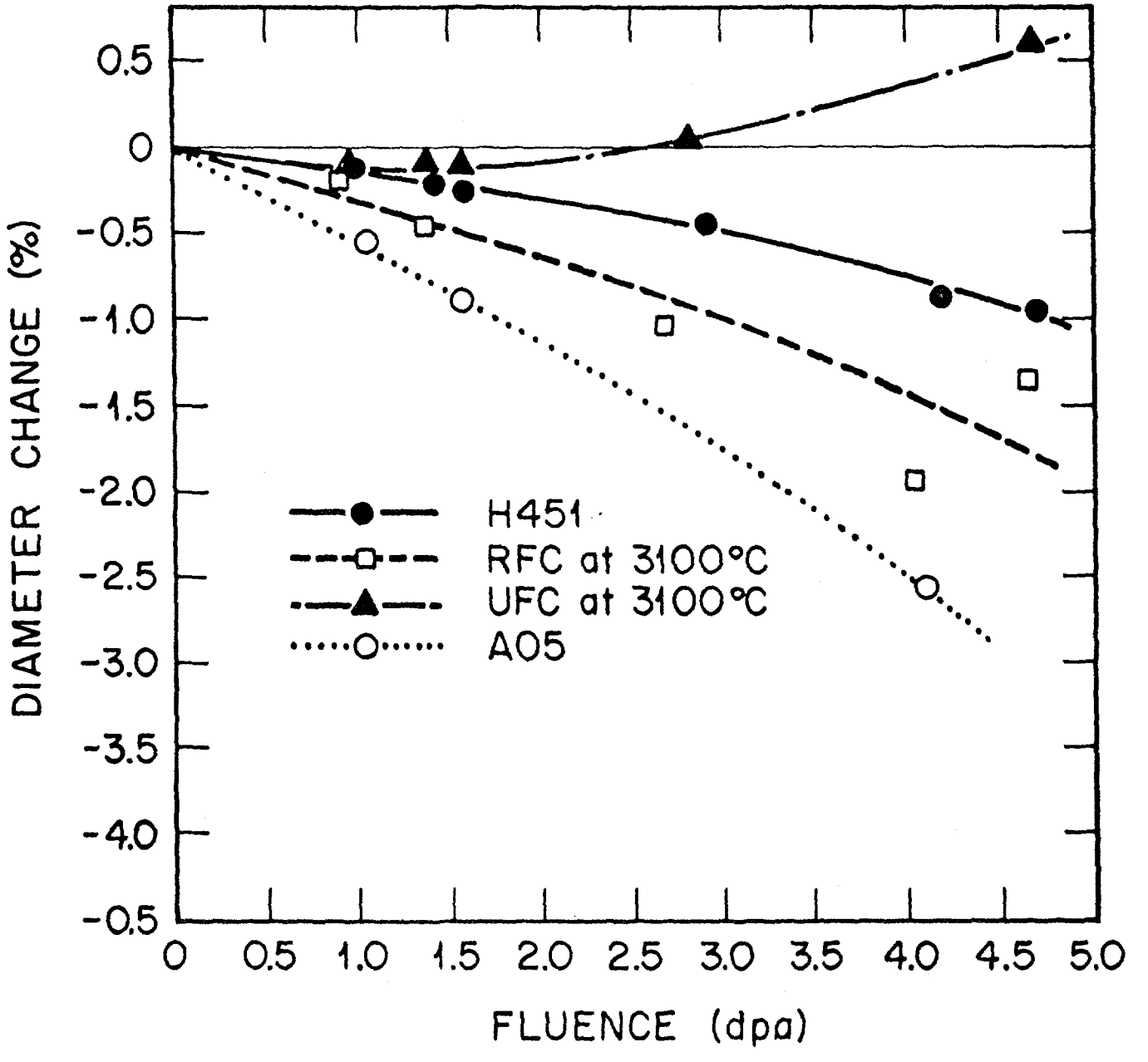
0.5
0
-0.5
-1.0
-1.5
-2.0
-2.5
-3.0
-3.5
-4.0
-0.5
DIAMETER CHANGE (%)
0
0.5
1.0
1.5
2.0
2.5
3.0
3.5
4.0
4.5
5.0
FLUENCE (dpa)
H451
RFC at 3100°C
UFC at 3100°C
A05

Fig. 5

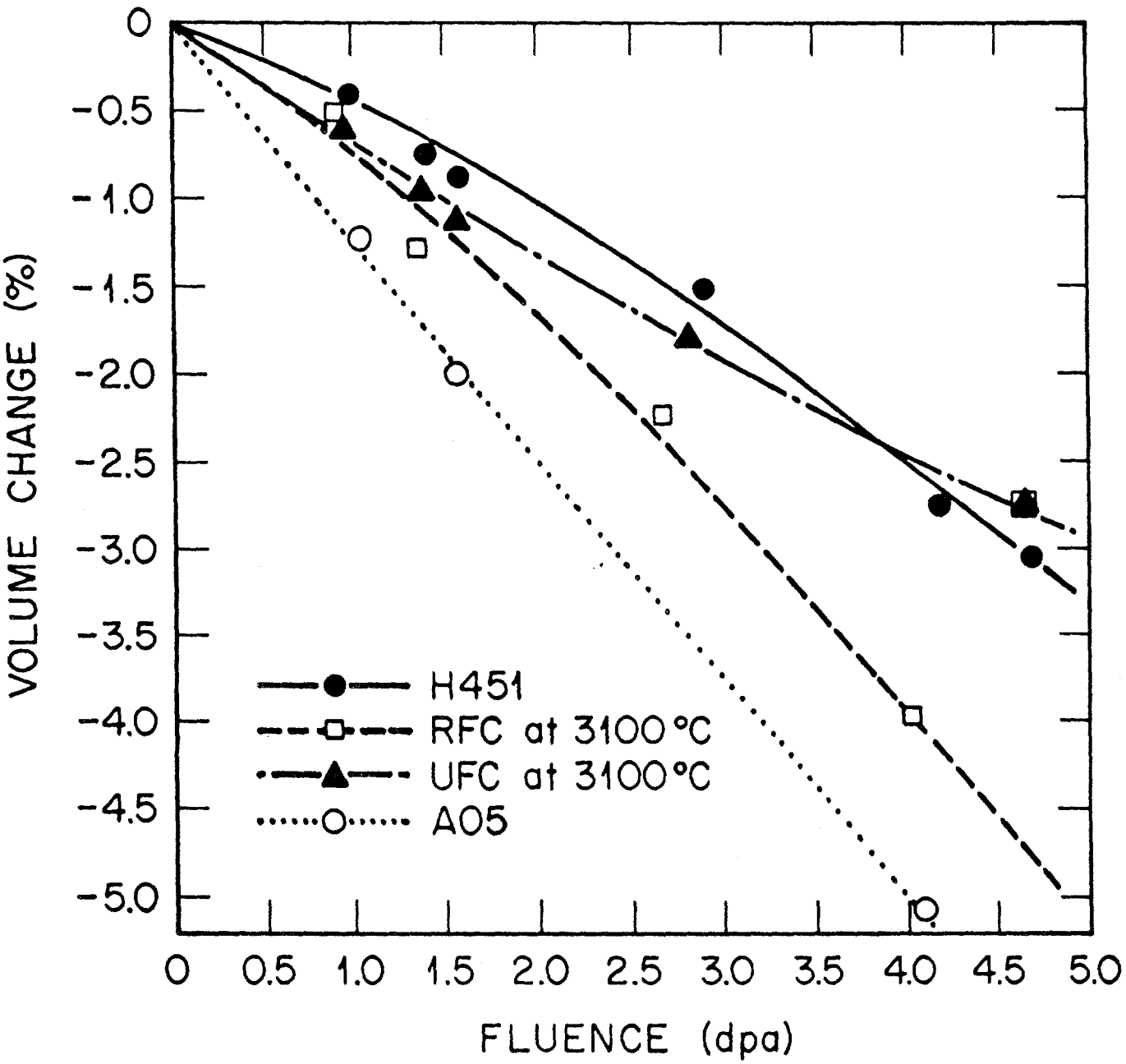
VOLUME CHANGE (%)
0
-0.5
-1.0
-1.5
-2.0
-2.5
-3.0
-3.5
-4.0
-4.5
-5.0
H451
RFC at 3100°C
UFC at 3100°C
A05
0
0.5
1.0
1.5
2.0
2.5
3.0
3.5
4.0
4.5
5.0
FLUENCE (dpa)

Fig. 6

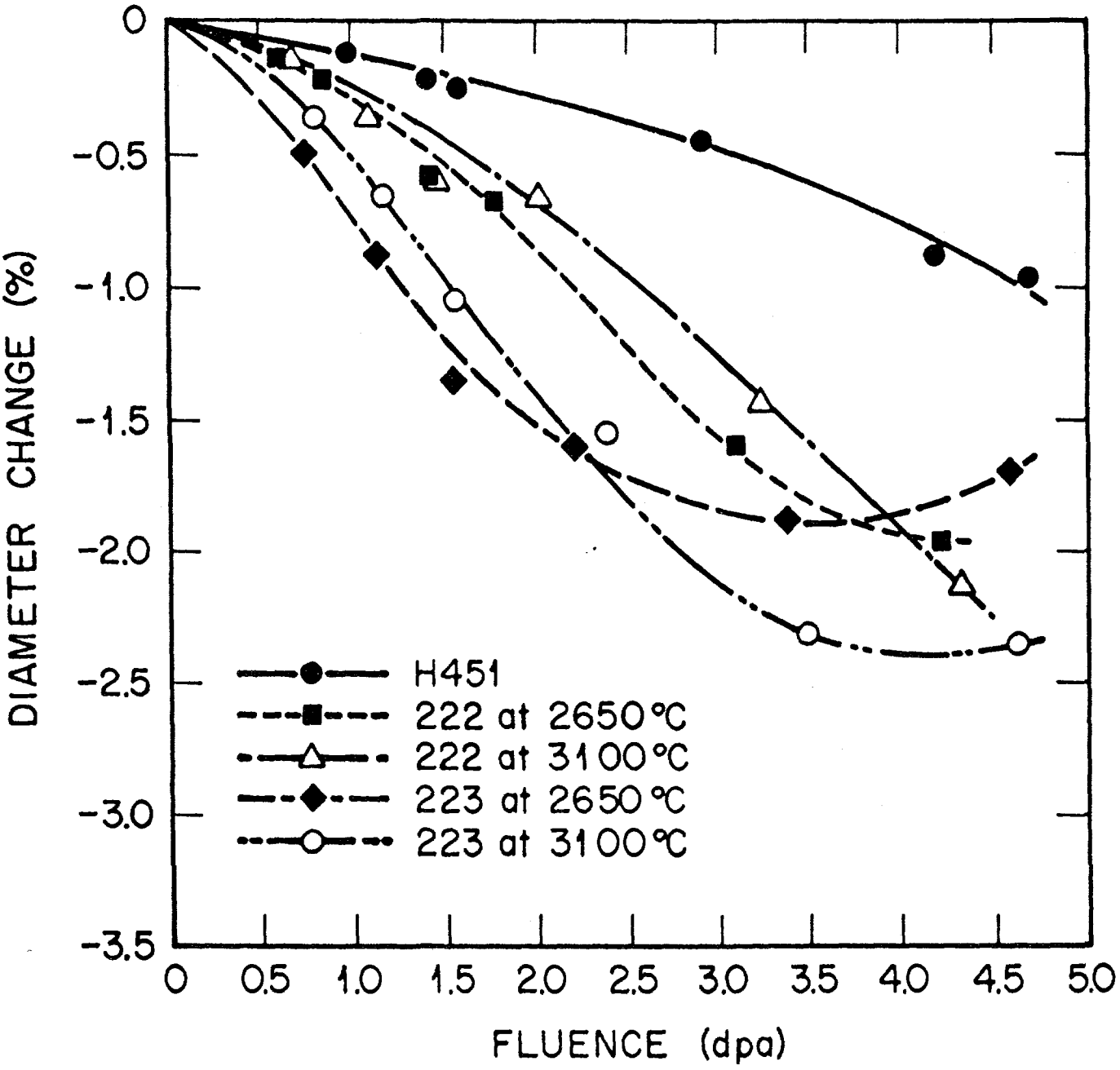
DIAMETER CHANGE (%)
0
-0.5
-1.0
-1.5
-2.0
-2.5
-3.0
-3.5
0
0.5
1.0
1.5
2.0
2.5
3.0
3.5
4.0
4.5
5.0
FLUENCE (dpa)
H451
222 at 2650°C
222 at 3100°C
223 at 2650°C
223 at 3100°C

Fig. 7

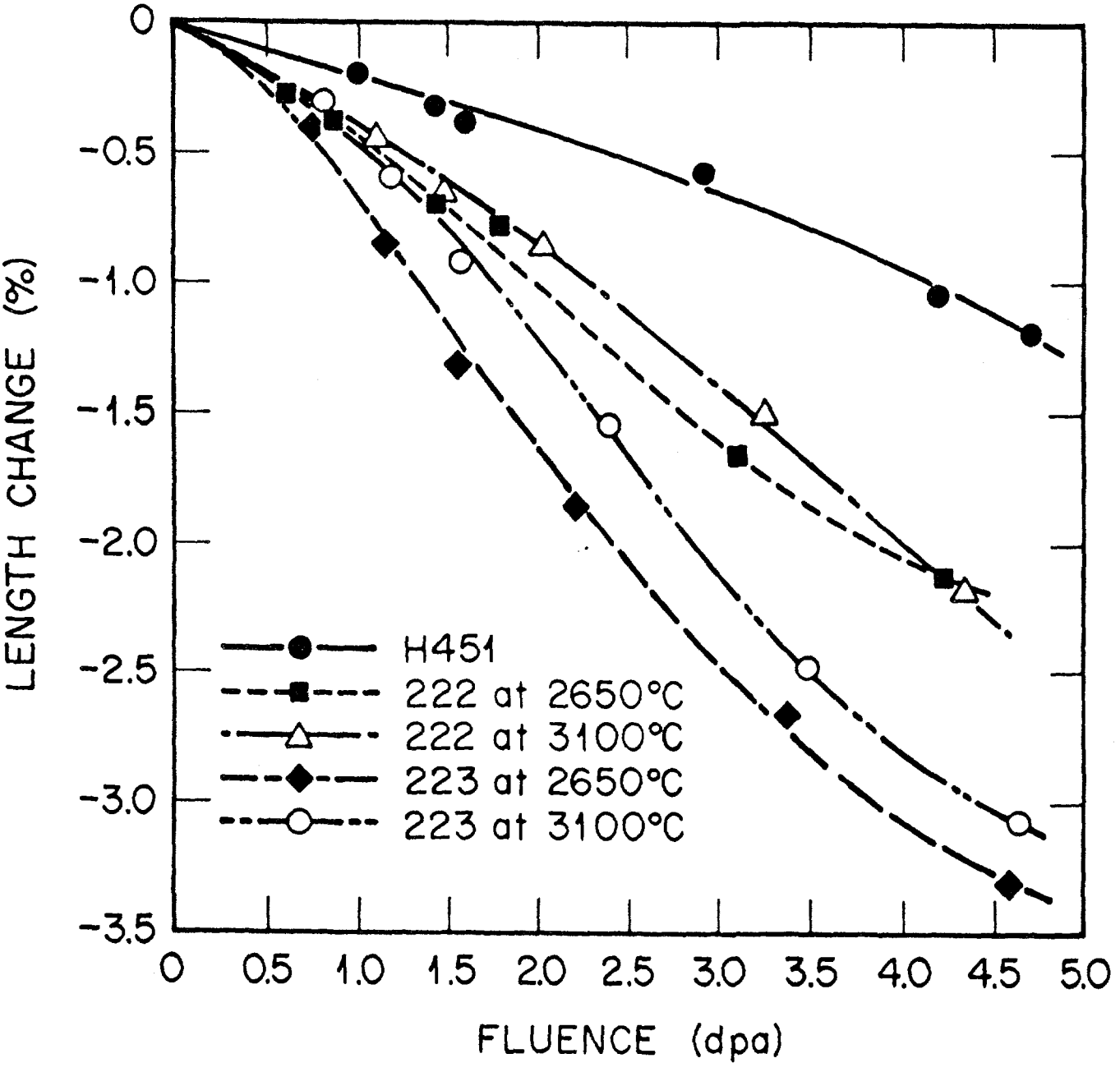
0
-0.5
-1.0
-1.5
-2.0
-2.5
-3.0
-3.5
LENGTH CHANGE (%)
0
0.5
1.0
1.5
2.0
2.5
3.0
3.5
4.0
4.5
5.0
FLUENCE (dpa)
H451
222 at 2650°C
222 at 3100°C
223 at 2650°C
223 at 3100°C

Fig. 8

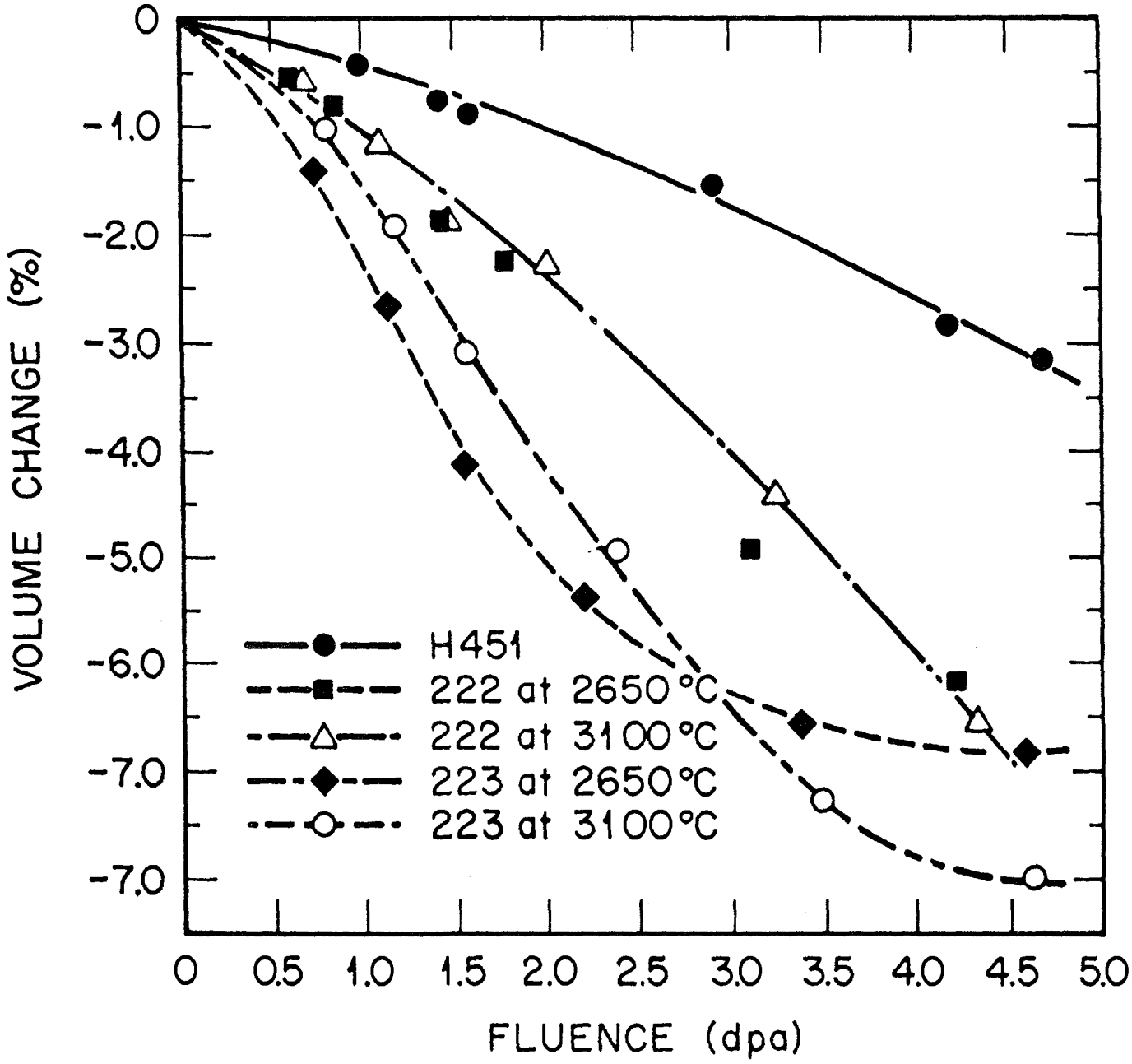
VOLUME CHANGE (%)
0
-1.0
-2.0
-3.0
-4.0
-5.0
-6.0
-7.0
-7.0
H451
222 at 2650 °C
222 at 3100 °C
223 at 2650 °C
223 at 3100 °C
0
0.5
1.0
1.5
2.0
2.5
3.0
3.5
4.0
4.5
5.0
FLUENCE (dpa)

Fig. 9

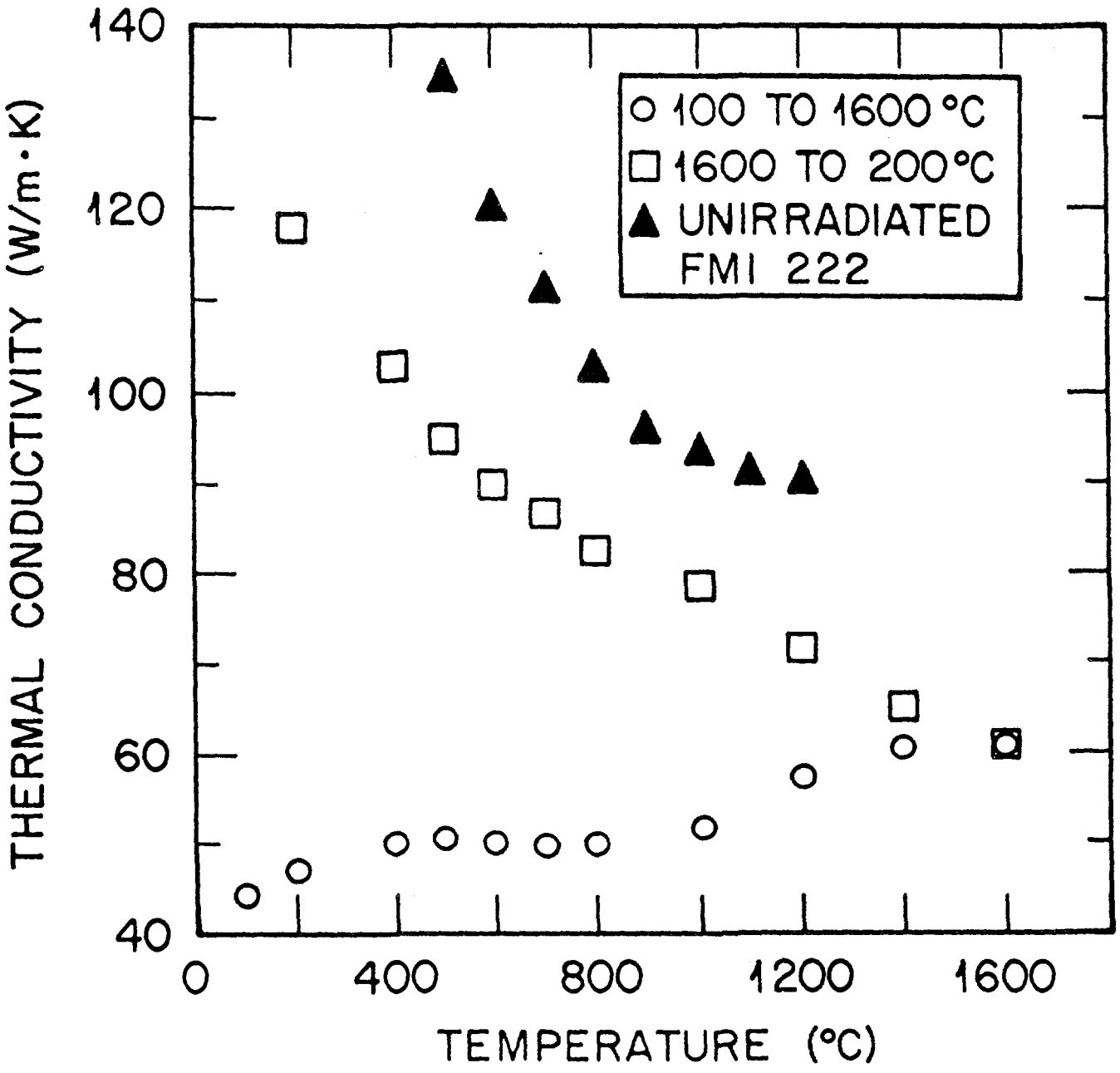
140
120
100
80
60
40
0
400
800
1200
1600
THERMAL CONDUCTIVITY (W/m·K)
TEMPERATURE (°C)
100 TO 1600 °C
1600 TO 200°C
UNIRRADIATED
FMI 222

Fig. 10

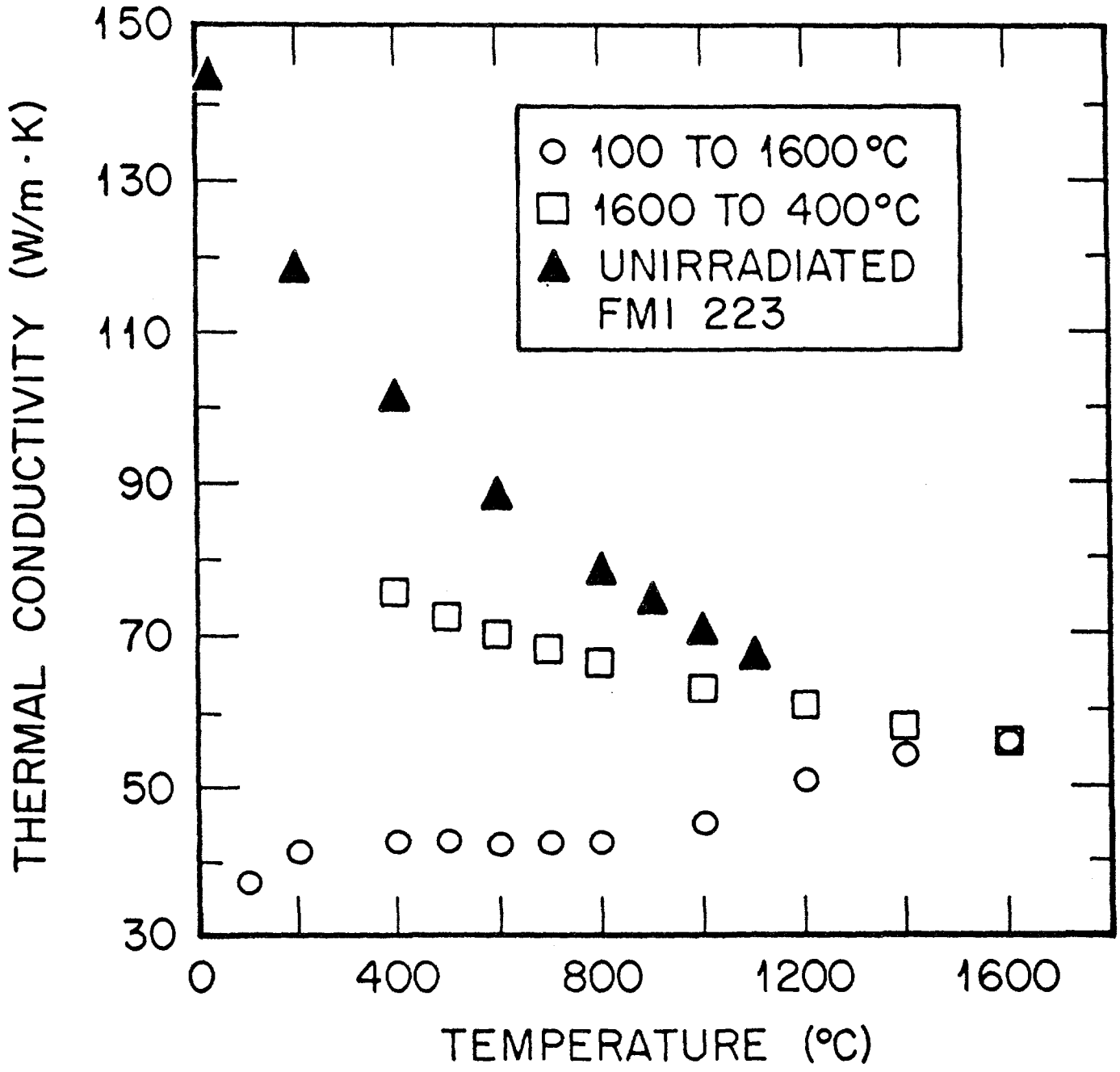
150
130
110
90
70
50
30
0
400
800
1200
1600
THERMAL CONDUCTIVITY (W/m·K)
TEMPERATURE (°C)
100 TO 1600°C
1600 TO 400°C
UNIRRADIATED
FMI 223

Fig. 11

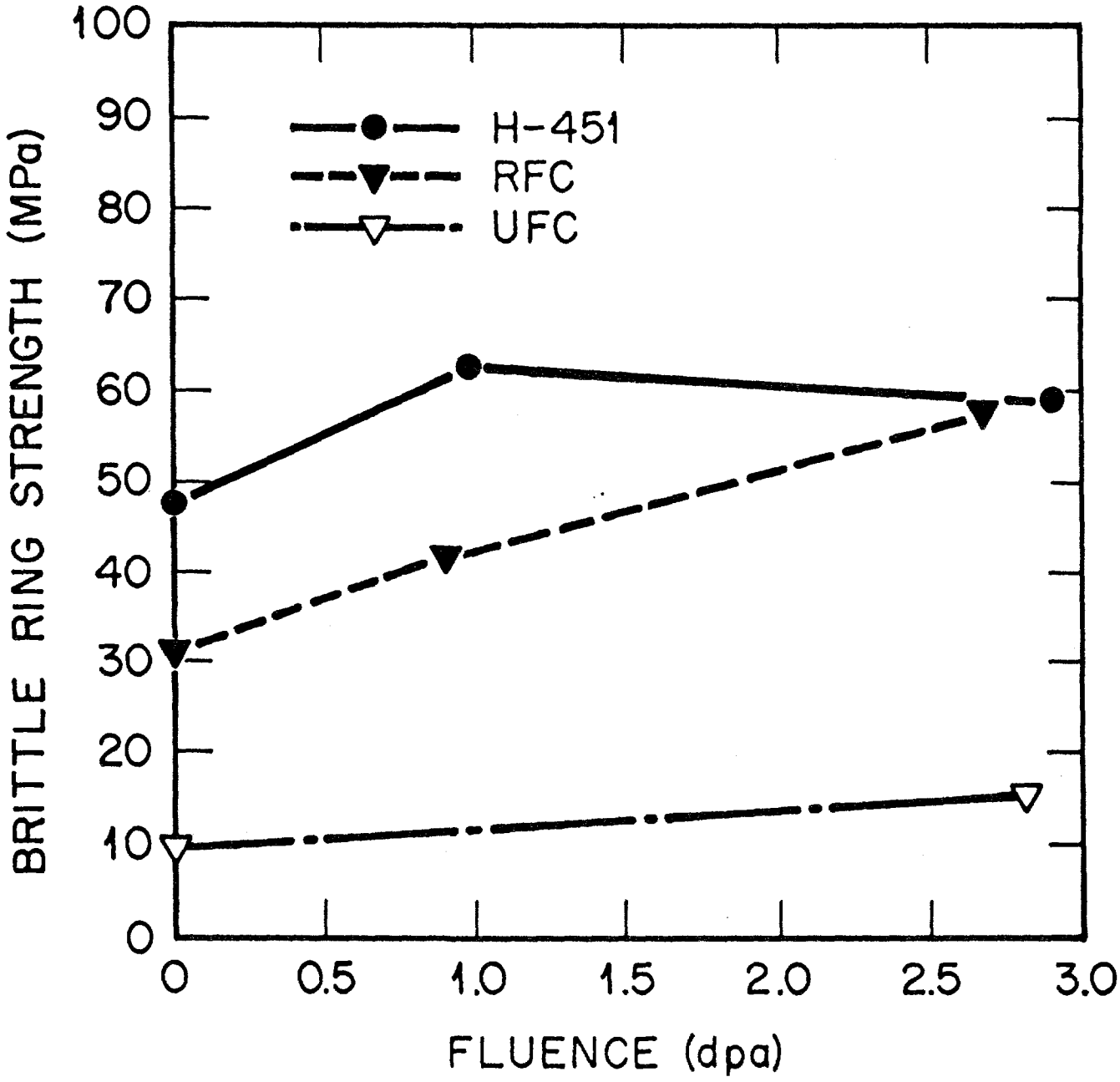
100
90
80
70
60
50
40
30
20
10
0
BRITTLE RING STRENGTH (MPa)
H-451
RFC
UFC
0
0.5
1.0
1.5
2.0
2.5
3.0
FLUENCE (dpa)

Fig. 12

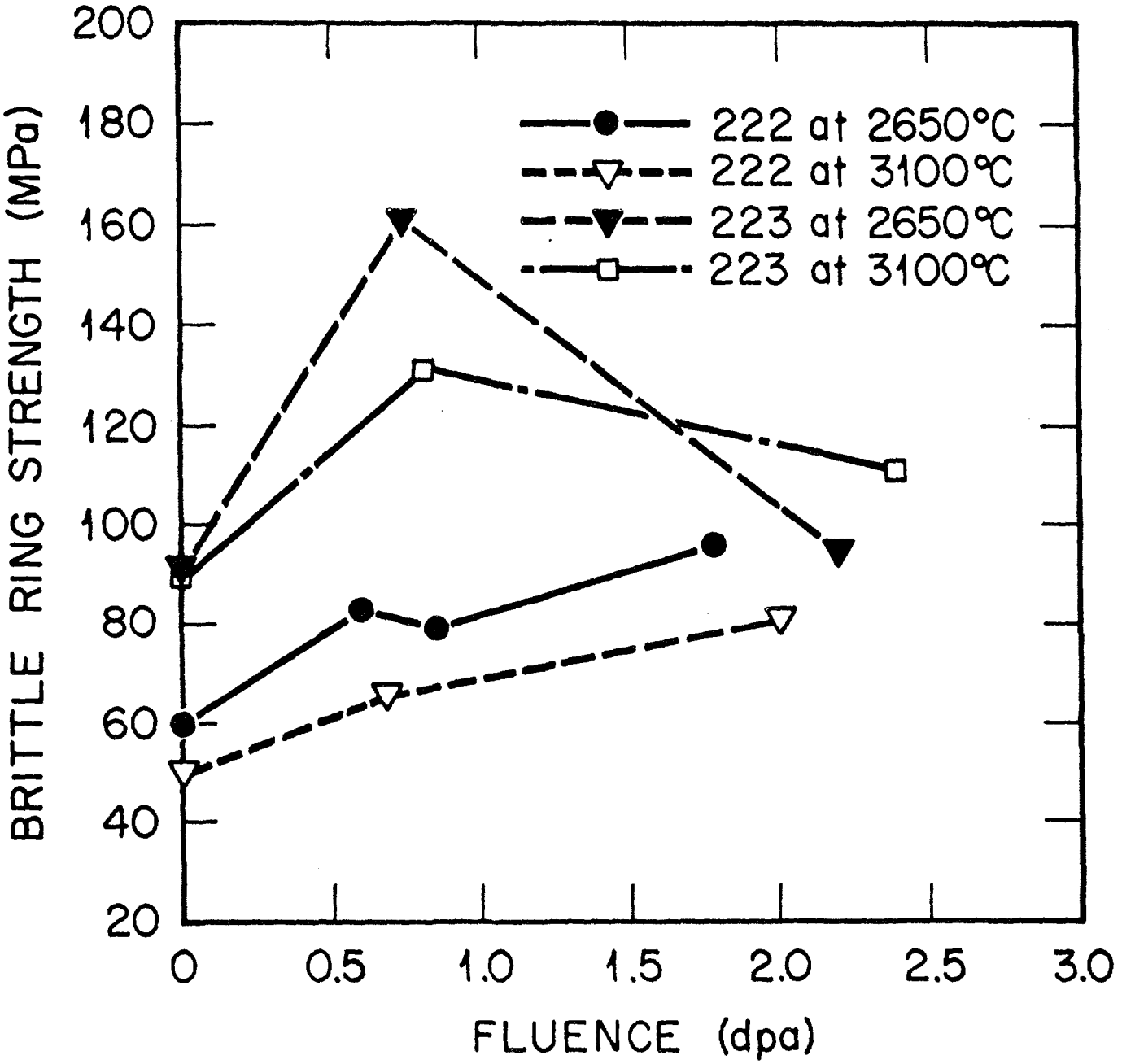
BRITTLE RING STRENGTH (MPa)
200
180
160
140
120
100
80
60
40
20
0
0.5
1.0
1.5
2.0
2.5
3.0
FLUENCE (dpa)
222 at 2650°C
222 at 3100°C
223 at 2650°C
223 at 3100°C

Fig. 13

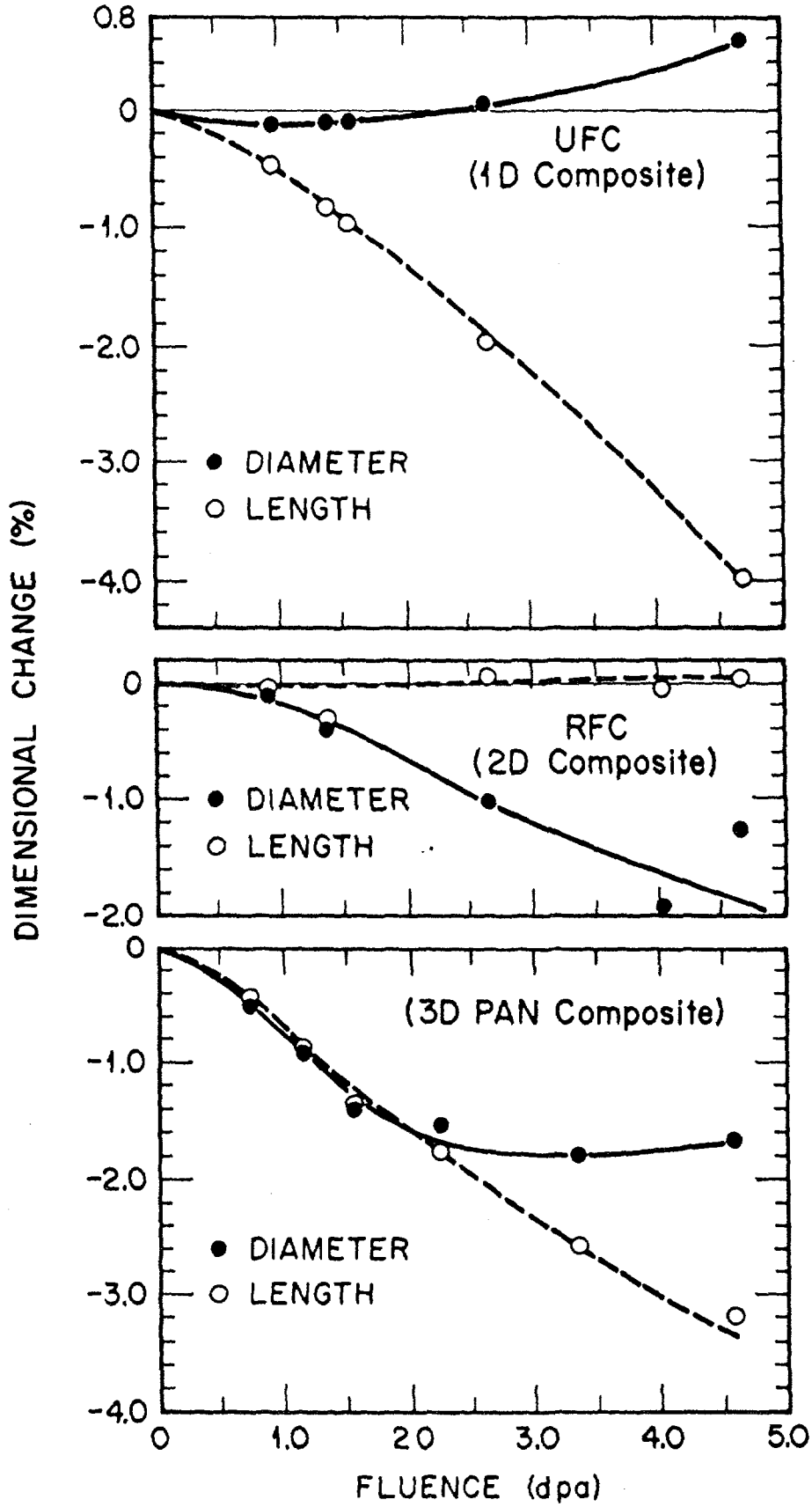
0.8
0
-1.0
-2.0
-3.0
-4.0
UFC
(1D Composite)
DIAMETER
LENGTH
0
-1.0
-2.0
RFC
(2D Composite)
DIAMETER
LENGTH
0
-1.0
-2.0
-3.0
-4.0
(3D PAN Composite)
DIAMETER
LENGTH
DIMENSIONAL CHANGE (%)
0
1.0
2.0
3.0
4.0
5.0
FLUENCE (dpa)

Fig. 14

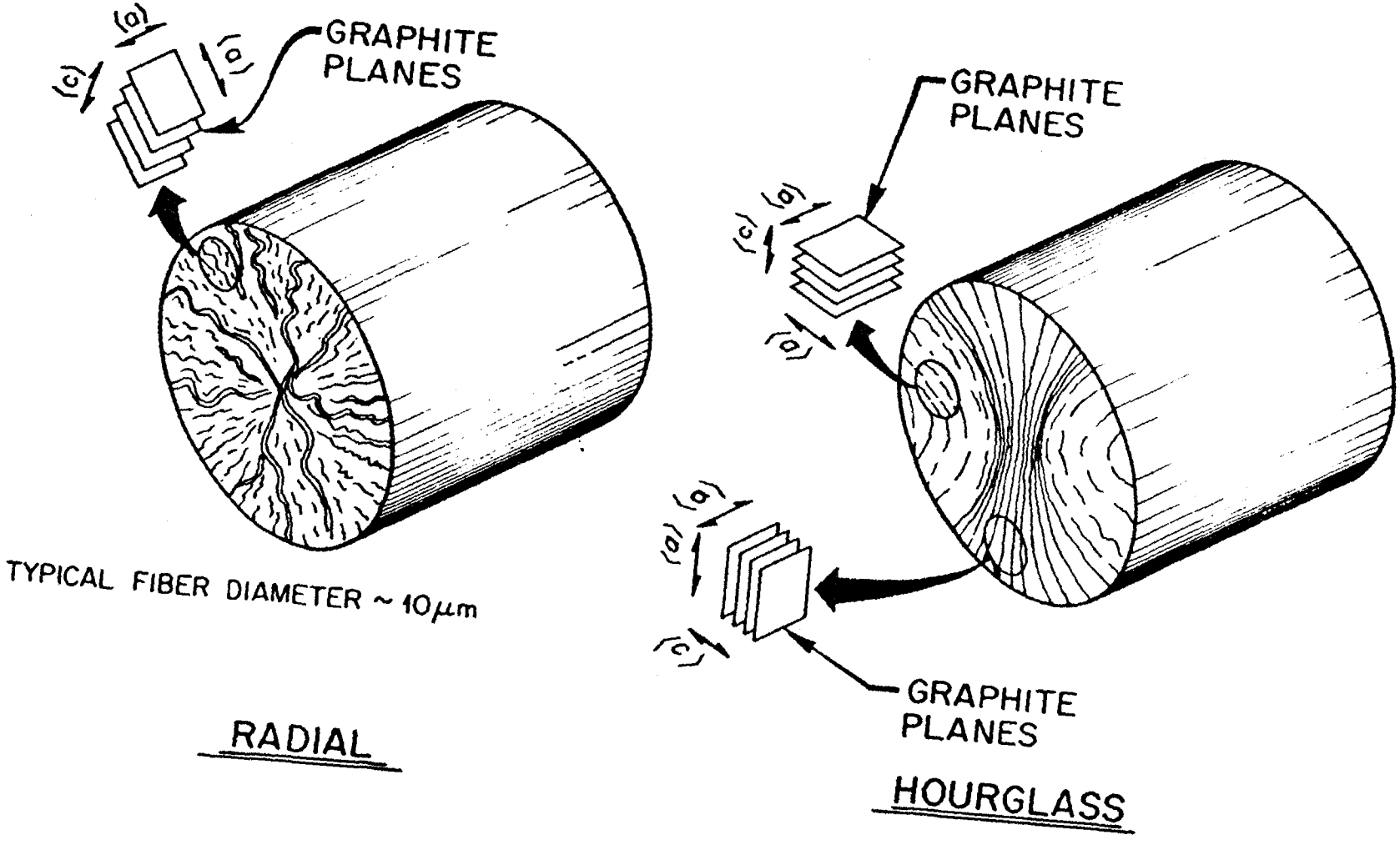


Fig. 15

G.M. Pennock et al.
CARBON, Vol. 31,
p. 596, 597 1993

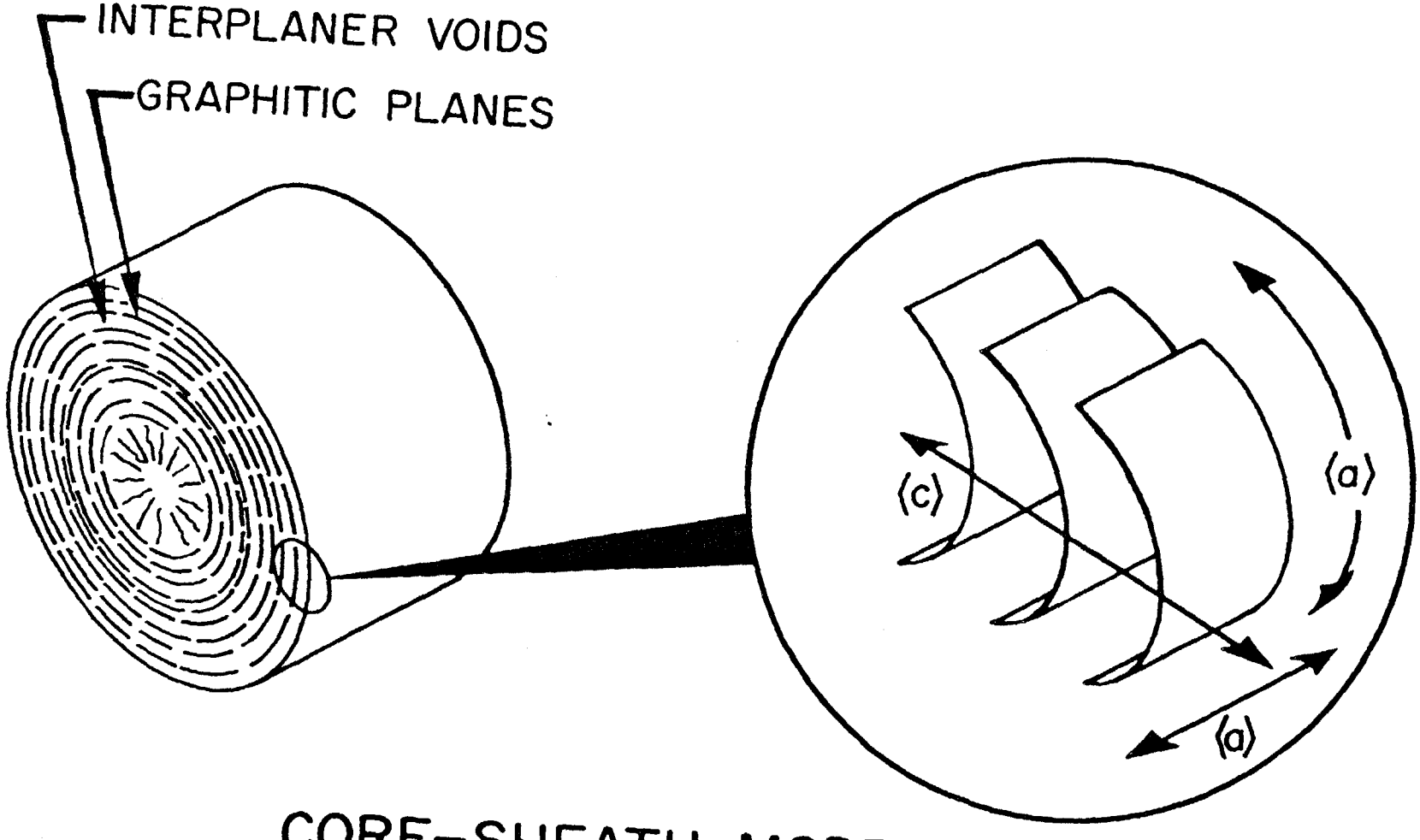


CORE-SHEATH MODEL

Fig. 16

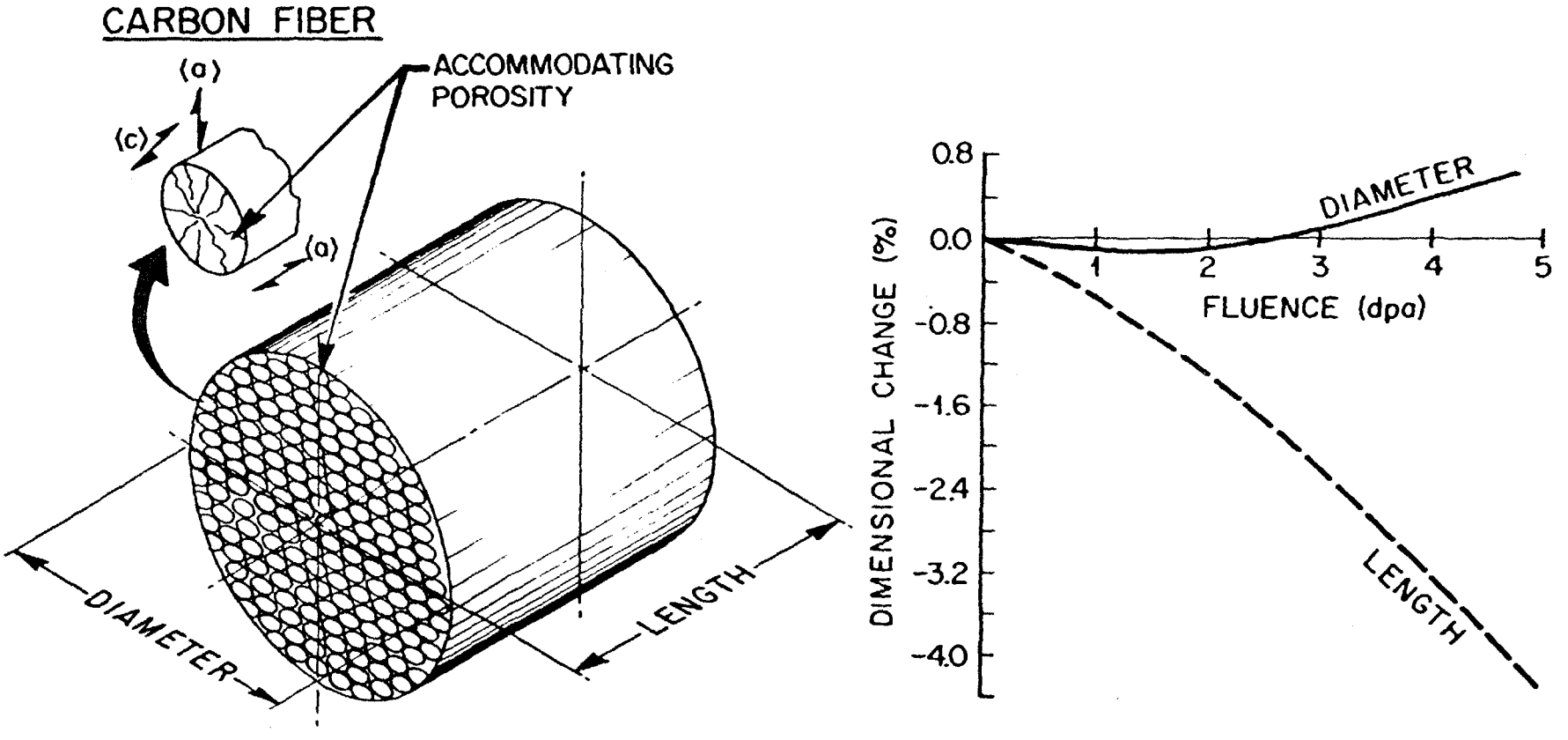


(a) CONTRACTION

(c) EXPANSION INITIALLY ACCOMMODATED BY POROSITY

Fig. 17

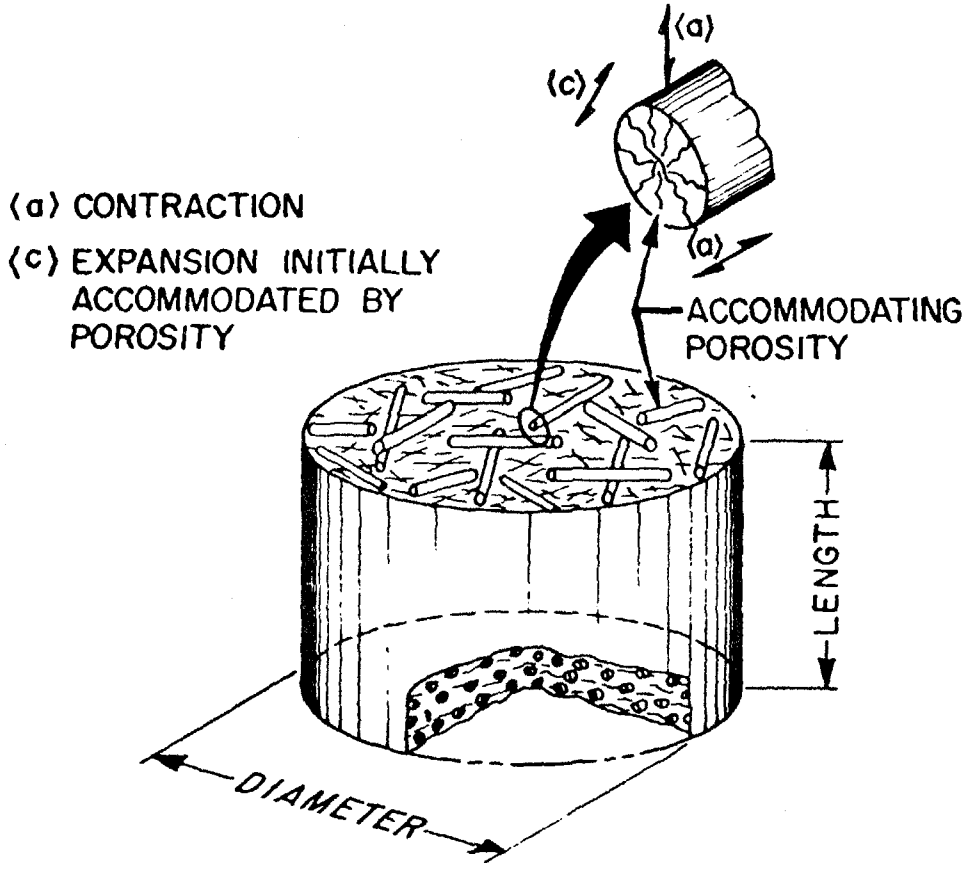
(a) CONTRACTION
(c) EXPANSION INITIALLY ACCOMMODATED BY POROSITY
(a)
(c)
(a)
ACCOMMODATING POROSITY
LENGTH
DIAMETER

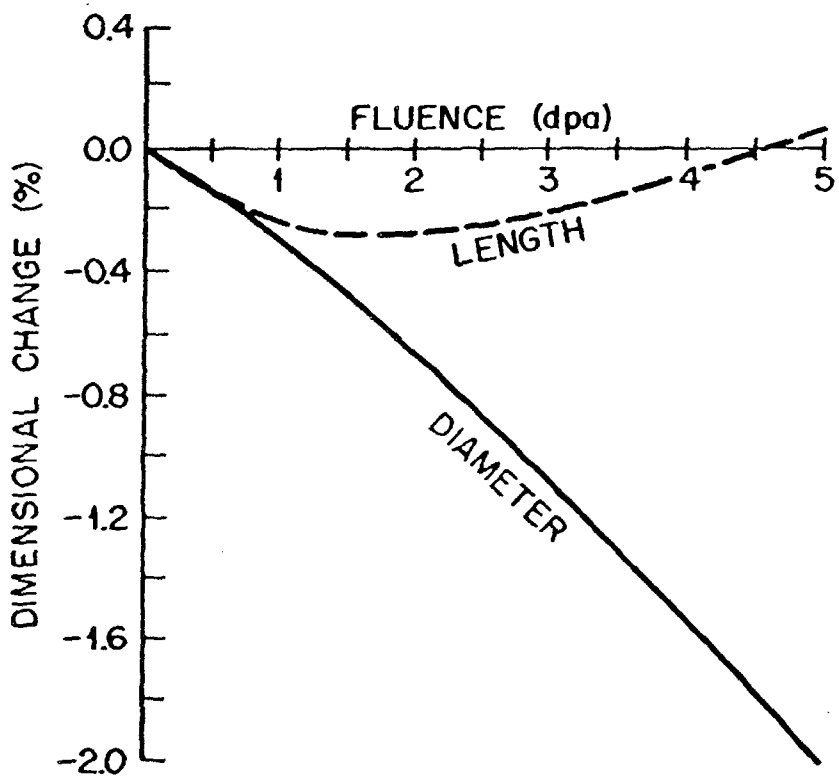
0.4
0.0
-0.4
-0.8
-1.2
-1.6
-2.0
DIMENSIONAL CHANGE (%)
FLUENCE (dpa)
1
2
3
4
5
LENGTH
DIAMETER

Fig. 18

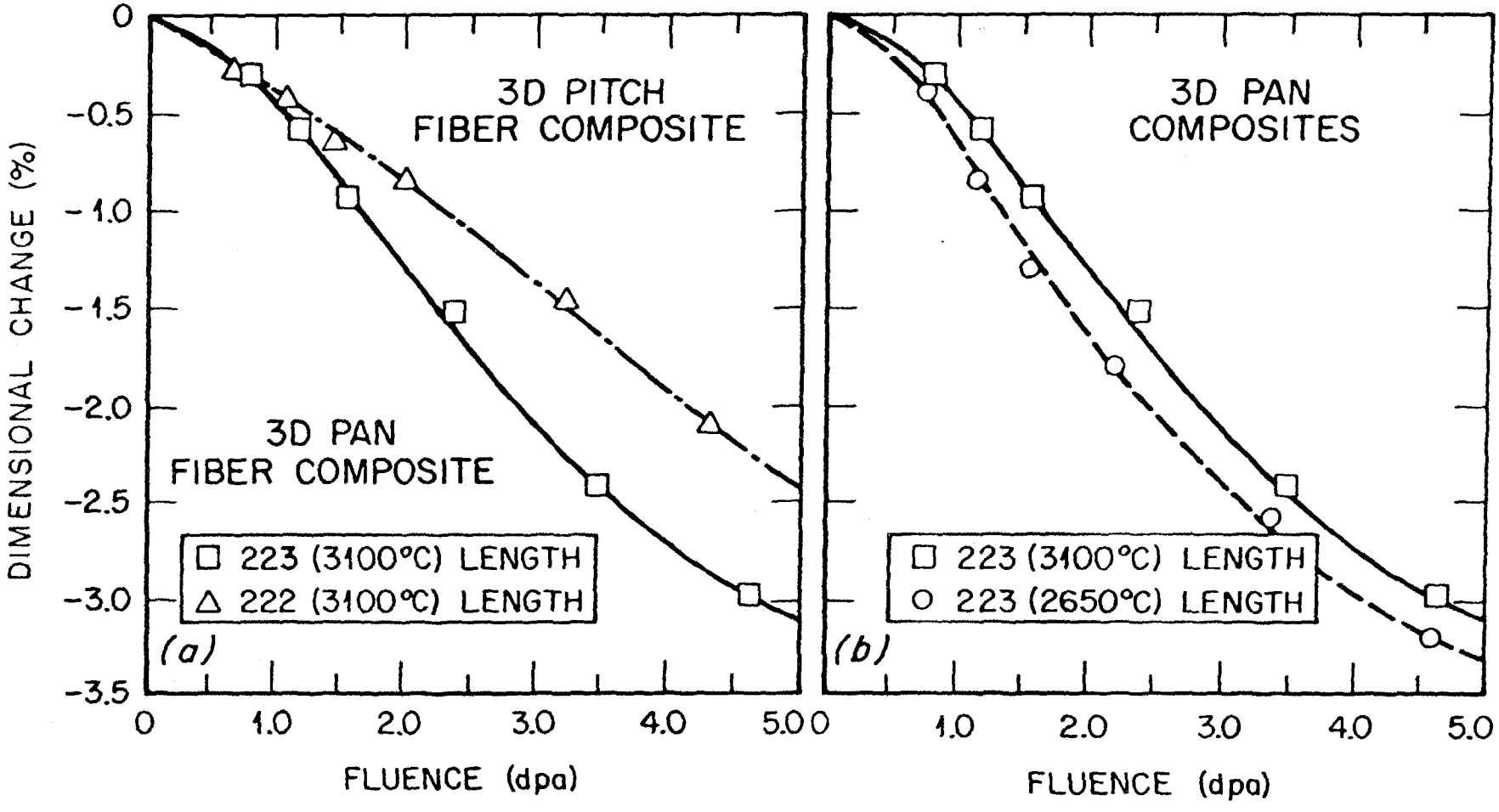


Fig. 19a

Fig 19b

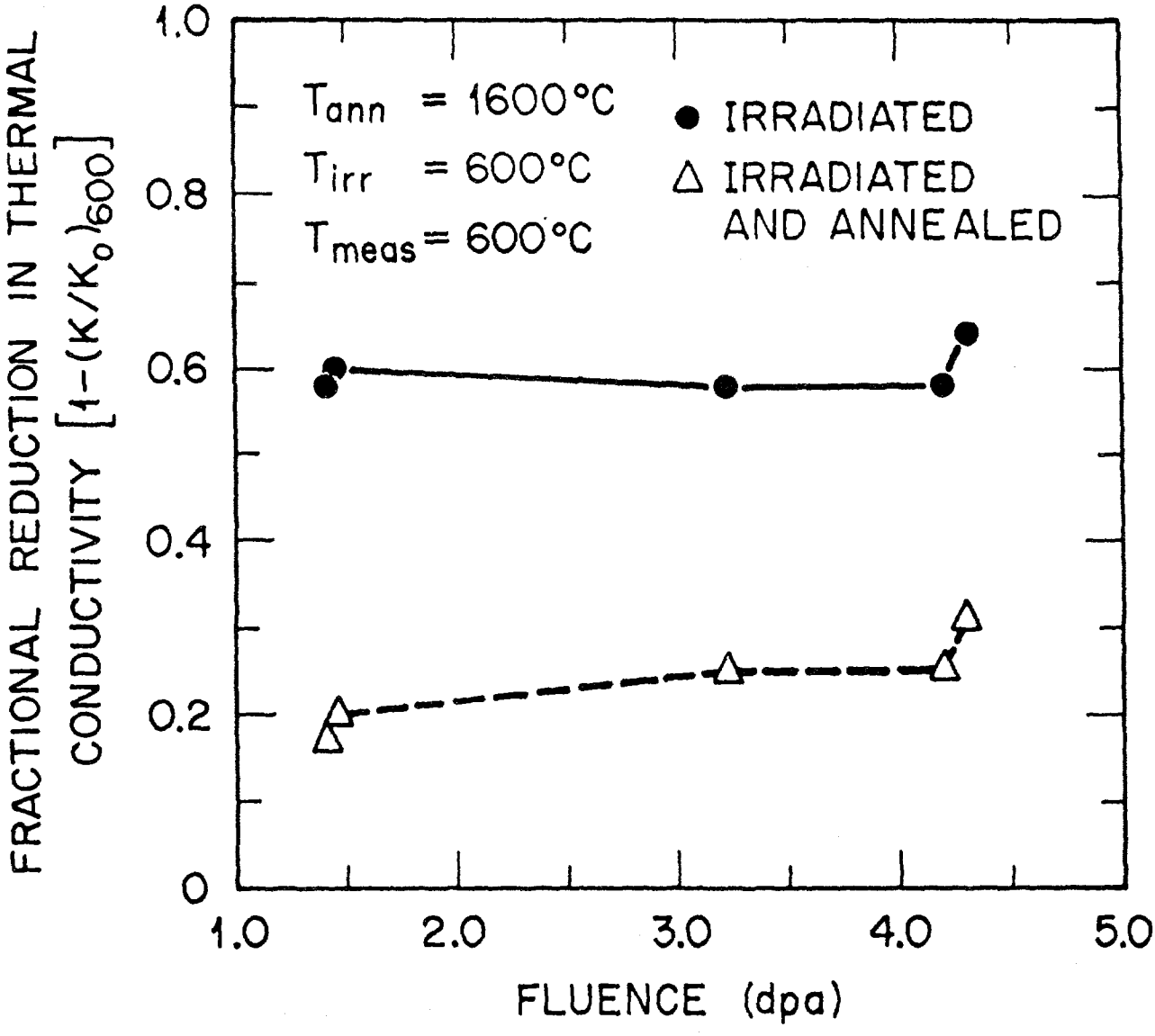
FRACTIONAL REDUCTION IN THERMAL CONDUCTIVITY [1-(K/K0)600]
1.0
0.8
0.6
0.4
0.2
0
Tann = 1600°C
Tirr = 600°C
Tmeas = 600°C
IRRADIATED
IRRADIATED AND ANNEALED
1.0
2.0
3.0
4.0
5.0
FLUENCE (dpa)

Fig. 20

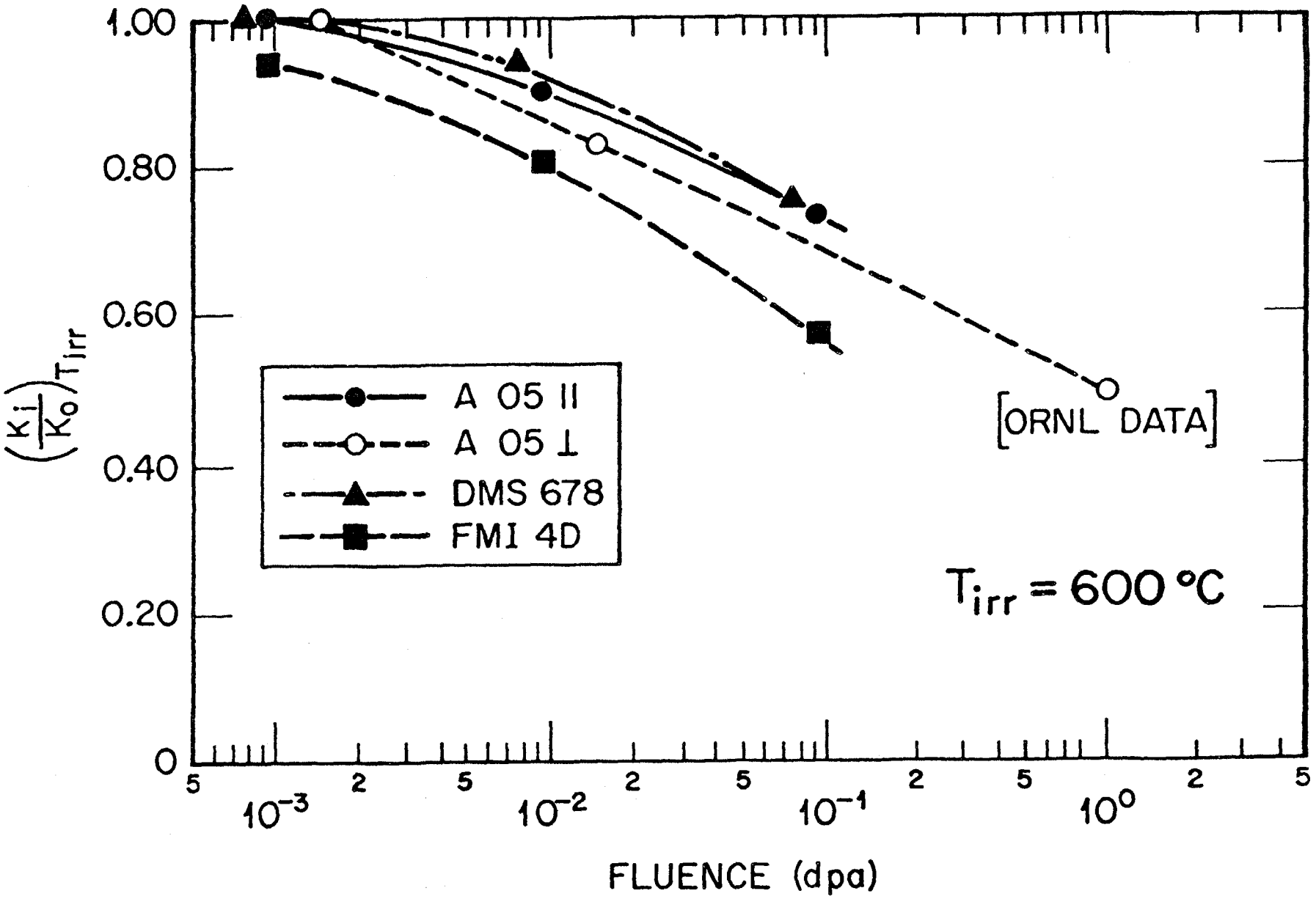
1.00
0.80
0.60
0.40
0.20
0
$\left(\frac{K_i}{K_o}\right)_{T_{irr}}$
A 05 II
A 05 ⊥
DMS 678
FMI 4D
[ORNL DATA]
$T_{irr}$ = 600 °C
5
2
5
2
5
2
5
2
5
$10^{-3}$
$10^{-2}$
$10^{-1}$
$10^{0}$
FLUENCE (dpa)

Fig. 21